A

ABSOLUTE AGE DETERMINATIONS: RADIOMETRIC

Richard W. Carlson
Department of Terrestrial Magnetism, Carnegie Institution of Washington, Washington, DC, USA

Definition

Radiometric dating uses the decay of naturally occurring radioactive elements to determine the absolute age of geologic events.

Introduction

Time is an essential datum in geology. Some geological processes, particularly those responsible for generating natural hazards, occur over time intervals that can be measured with conventional clocks. Most geologic processes, however, occur on timescales beyond human experience – thousands, millions, and even billions of years (see *Continental Drift*; *Continental Rifts*; *Geodynamics*; *Lithosphere, Continental*; *Paleomagnetism, Magnetostratigraphy*; *Paleoseismology*; *Plate Tectonics, Precambrian*). For these, the chronometer of choice is radiometric dating, where the decay of naturally occurring radioactive elements is translated into time (Dickin, 2005; Faure and Mensing, 2005). In its application to geochronology, the most important aspect of radioactive decay is that it occurs at a known, constant rate, independent of environmental factors such as changing temperature and pressure, at least within the ranges of these parameters found outside the interior of stars.

Only 10 years after the discovery of radioactivity, the renowned physicist Ernest Rutherford measured the amount of helium in a uranium ore and derived an age of 500 million years for the ore (Rutherford, 1906). By 1913, radioactive dating of rocks had made important inroads into geologic investigations of Earth history (Holmes, 1913). The discovery of isotopes, also in 1913, and the improvement of the instruments used to measure their abundance (mass spectrometers) over the next decades, allowed radioactive dating to be applied to an increasingly broad range of natural materials, and hence, geologic processes. This, in turn, facilitated the transition of isotopic measurements from physics to geology departments and established radiometric geochronology as a tool of widespread use in the geosciences in the years following World War II.

Radioactivity and the systematics of its use as a chronometer

Radiometric dating is based on the principle of nuclear transmutation, common to alchemy. Some elements have isotopes whose nuclei contain an unstable number of neutrons and protons. The instability is most often remedied by the ejection of material from the nucleus. Alpha decay involves the ejection of two protons and two neutrons (a 4-helium (^{4}He) nucleus or alpha particle). Beta decay occurs through loss of an electron from the nucleus, turning a neutron into a proton. Another form of radioactive decay involves the capture of an electron from those surrounding the nucleus, turning a proton into a neutron. All forms of radioactive decay also release energy, and are thus a heat source in Earth's interior (see *Radiogenic Heat Production of Rocks*; *Energy Budget of the Earth*). The result of radioactive decay is that an isotope of one element is transformed into an isotope of another element. While the path from lead to gold does not occur naturally, if one waits long enough, radioactive decay will eventually transform all uranium and thorium into lead.

Table 1 lists the major radioactive nuclides that have been used for dating various geologic events. Naturally

Harsh K. Gupta (ed.), *Encyclopedia of Solid Earth Geophysics*, DOI 10.1007/978-90-481-8702-7,
© Springer Science+Business Media B.V. 2011

Absolute Age Determinations: Radiometric, Table 1 Radioactive elements commonly used for absolute age determinations

Parent isotope	Production mechanism	Daughter isotope	Half-Life (Million years)
7-Berylium (^{7}Be)	Cosmogenic	7-Lithium (^{7}Li)	53 days
210-Lead (^{210}Pb)	Uranium decay	210-Bismuth (^{210}Bi)	22.3 years
226-Radium (^{226}Ra)	Uranium decay	222-Radon (^{222}Rn), ^{4}He	1,622 years
14-Carbon (^{14}C)	Cosmogenic, Bomb	14-Nitrogen (^{14}N)	5,730 years
231-Protactinium (^{231} Pa)	Uranium Decay	227-Thorium (^{227}Th), ^{4}He	0.033
234-Uranium (^{234}U)	Uranium Decay	230-Thorium (^{230}Th), ^{4}He	0.25
36-Chlorine (^{36}Cl)	Cosmogenic, Bomb	36-Argon (^{36}Ar)	0.31
26-Aluminum (^{26}Al)	Cosmogenic, Stellar	26-Magnesium (^{26} Mg)	0.73
230-Thorium (^{230}Th)	Uranium Decay	226-Radium (^{226}Ra), ^{4}He	0.75
60-Iron (^{60}Fe)	Stellar	60-Nickel (^{60}Ni)	1.5
10-Berylium (^{10}Be)	Cosmogenic, Stellar	10-Boron (^{10}B)	1.6
53-Manganese (^{53}Mn)	Cosmogenic, Stellar	53-Chromium (^{53}Cr)	3.7
107-Paladium (^{107}Pd)	Stellar	107-Silver (^{107}Ag)	6.5
182-Hafnium (^{182}Hf)	Stellar	182-Tungsten (^{182} W)	9
129-Iodine (^{129}I)	Stellar, Cosmogenic	129-Xenon (^{129}Xe)	15.7
244-Plutonium (^{244}Pu)	Stellar	Various fission products	80
146-Samarium (^{146}Sm)	Stellar	142-Neodymium (^{142}Nd)	103
235-Uranium (^{235}U)	Stellar	207-Lead (^{207}Pb), ^{4}He	704
40-Potassium (^{40} K)	Stellar	40-Argon (^{40}Ar) 40-Calcium (^{40}Ca)	1,270
238-Uranium (^{238}U)	Stellar	206-Lead (^{206}Pb), ^{4}He	4,469
232-Thorium (^{232}Th)	Stellar	208-Lead (^{208}Pb), ^{4}He	14,010
176-Lutetium (^{176}Lu)	Stellar	176-Hafnium (^{176}Hf)	35,700
187-Rhenium (^{187}Re)	Stellar	187-Osmium (^{187}Os)	41,600
87-Rubidium (^{87}Rb)	Stellar	87-Strontium (^{87}Sr)	48,800
147-Samarium (^{147}Sm)	Stellar	143-Neodymium (^{143}Nd), ^{4}He	106,000
190-Platinum (^{190}Pt)	Stellar	186-Osmium (^{186}Os)	450,000

occurring radioactive isotopes are produced through four mechanisms:

1. Stellar nucleosynthesis where the very high temperatures and pressures present in stellar interiors fuse nuclei, creating new elements (Truran and Heger, 2005).
2. Some radioactive elements decay into other radioactive elements. For example, 238-uranium requires eight alpha decays and six beta decays before it reaches stable 206-lead. Along the way, the decay steps include some isotopes with long enough decay lives to be useful in geochronology. These include ^{234}U, ^{230}Th, ^{226}Ra, ^{222}Rn, and ^{210}Pb.
3. High-energy cosmic ray particles collide with atoms in Earth's atmosphere or surface rocks with enough energy to cause nuclear reactions. For example, 14-carbon is created when 14-nitrogen in the atmosphere captures a neutron released by a cosmic ray interaction with some other atom. Other cosmic-ray-produced nuclides include ^{10}Be and ^{26}Al that are made by spallation, which occurs when an energetic cosmic ray proton simply breaks off a fragment from the nucleus of an atom with which it collides. Radioactive isotopes produced in these reactions are known as cosmogenic isotopes.
4. Above-ground detonations of nuclear bombs introduced into the environment substantial quantities of a number of radioactive species that have been used to investigate a number of atmosphere – Earth's surface exchange processes, and for tracing ocean water circulation.

The probability that a radioactive isotope will decay over any time interval is described by the equation:

$$-dN/dt = \lambda N \quad (1)$$

where N is the number of atoms of the radioactive species (parent isotope), t is time, and λ is the rate constant of the decay. Rate constants often are converted to "half-life"; the time needed for half of the radioactive species to decay. The half-life of a radioactive species is equal to ln(2)/λ. Integrating Equation 1 gives:

$$N = N_0 e^{-\lambda t} \quad (2)$$

where N_0 is the number of atoms present when t = 0. This equation can be used to determine ages if one has independent information on the initial abundance of the parent isotope. For example, in ^{14}C dating, if one assumes that the ratio of ^{14}C to stable ^{12}C is constant in the atmosphere, then one need only measure the present day ^{14}C/^{12}C ratio in a material that obtained its carbon from the atmosphere and use Equation 2 in order to determine the material's age. The assumption of a constant atmospheric ^{14}C/^{12}C

ratio is now known to be invalid because the production rate of ^{14}C in the atmosphere depends on issues as diverse as sunspot activity and the varying strength of Earth's magnetic field (see *Paleomagnetic Field Intensity*). Various schemes have been used to correct ^{14}C chronology for variations in the atmospheric ^{14}C production rate including comparison with the carbon in tree rings dated simply by counting the annual growth rings (Friedrich et al., 1999) or, for longer time intervals, to growth rings in corals dated with ^{230}Th and ^{234}U (Fairbanks et al., 2005). Although the variations in ^{14}C production rate complicate ^{14}C dating, they potentially provide information on the variability of Earth's magnetic field, or sunspot activity, and how these parameters may affect Earth's climate (Bard and Frank, 2006).

Because the initial abundance of the parent isotope generally is not known, most radioactive dating schemes measure the increase in the abundance of the decay product (daughter). If no atoms are lost, the abundance of the daughter isotope (D) increases with time at the rate described by:

$$D = N_0 - N = N\left(e^{\lambda t} - 1\right) \tag{3}$$

Thus, in an ideal situation where, for example, a mineral forms that contains radioactive ^{40}K, but no ^{40}Ar, the age of the mineral can be determined simply by measuring the abundance of ^{40}K (N) and ^{40}Ar (D) in the mineral after some decay interval has passed. In nature, perfect separation of parent from daughter isotope is rare, so if some atoms of the decay product are present initially (D_0), then:

$$D = D_0 + N\left(e^{\lambda t} - 1\right) \tag{4}$$

Because mass spectrometers can measure isotopic ratios of some elements to precisions of 0.0005% whereas elemental abundances can only be determined to about 0.1–1% precision, Equation 4, using the ^{238}U-^{206}Pb decay scheme as an example, can be expressed as:

$$\left(^{206}Pb/^{204}Pb\right)_m = \left(^{206}Pb/^{204}Pb\right)_0 + \left(^{238}U/^{204}Pb\right)_m\left(e^{\lambda t} - 1\right) \tag{5}$$

where "m" stands for the measured ratio and λ is the decay constant of ^{238}U. Pb-204 is a stable isotope of lead. If two or more samples with different U/Pb ratios are formed at the same time with the same initial Pb isotope composition ($(^{206}Pb/^{204}Pb)_0$), after some time has passed, plotting the measured $^{206}Pb/^{204}Pb$ for each sample against its $^{238}U/^{204}Pb$ ratio will produce a line, called an isochron, whose slope and y-intercept correspond to $(e^{\lambda t} - 1)$, and the initial $^{206}Pb/^{204}Pb$ ratio, respectively (Figure 1a). Thus, the slope of an isochron provides the time when the samples on the line had the same Pb isotope composition. The U–Pb system is unique in that it contains two isotopes of U that decay into two isotopes of Pb.

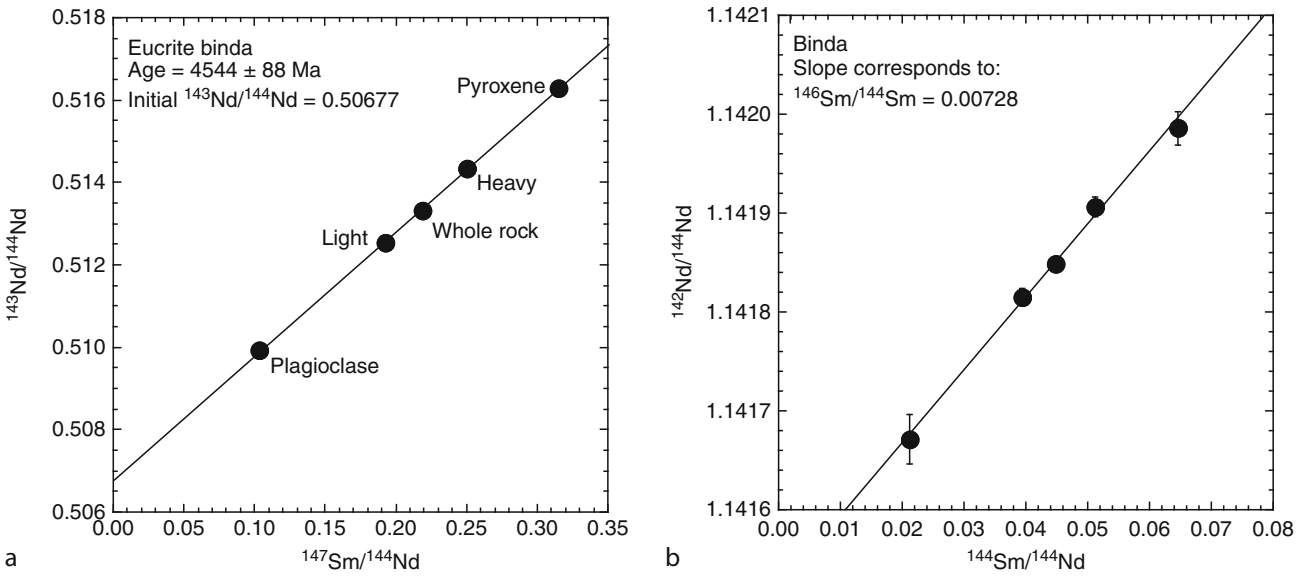

Absolute Age Determinations: Radiometric, Figure 1 Isochron diagrams for the long-lived ^{147}Sm–^{143}Nd and short-lived, now extinct, ^{146}Sm–^{144}Nd systems. The data shown are for minerals separated from the Binda eucrite, a type of meteorite that is a volcanic rock erupted on some small planetesimal. The meteorite consists primarily of the minerals plagioclase and pyroxene, which have different ratios of Sm to Nd when they form, but the same initial Nd isotopic composition. As Sm decays, it changes the isotopic composition of Nd. Using an equation similar to 5, the slope on the ^{147}Sm-^{143}Nd diagram directly provides the age of the sample, but on the ^{146}Sm-^{142}Nd diagram the slope provides the initial abundance of ^{146}Sm (actually the $^{146}Sm/^{144}Sm$ ratio as illustrated in an equation analogous to Equation 8). Data from Boyet et al. (2010).

Thus, an analogous Equation 5 can be written for the decay of ^{235}U to ^{207}Pb. More importantly, the two equations can be combined to give:

$$\frac{\left(^{207}Pb/^{204}Pb\right)_m - \left(^{207}Pb/^{204}Pb\right)_0}{\left(^{206}Pb/^{204}Pb\right)_m - \left(^{206}Pb/^{204}Pb\right)_0} = \frac{\left(^{235}U/^{238}U\right)\left(e^{\lambda_5 t} - 1\right)}{\left(e^{\lambda_8 t} - 1\right)} \quad (6)$$

where λ_5 and λ_8 are the decay constants for ^{235}U and ^{238}U, respectively. Because the $^{235}U/^{238}U$ ratio is nearly constant in nature at any given time, this equation allows an age to be determined from measurements of lead isotopic composition alone, without the need for concentration determinations of U or Pb. Such ages, called Pb–Pb ages, are obtained by plotting $(^{207}Pb/^{204}Pb)_m$ versus $(^{206}Pb/^{204}Pb)_m$, which will produce a line for two or more samples whose slope is equal to the right hand side of Equation 6. This equation can then be solved numerically to determine "t", the time when the samples formed.

A very active application of radiometric chronology uses the variety of short-lived (half-lives of 10^5–10^8 year) radionuclides that were present when the solar system formed, but have long since decayed away (Carlson and Boyet, 2009). For these systems, the "t" in Equation 2 cannot be referenced to today because $e^{-\lambda t}$ would always be close to zero. Instead, the "t" for these extinct systems must be a time interval referenced to a time when the parent isotope still existed. In this case, using the decay of ^{26}Al to ^{26}Mg as an example, Equation 5 can be rewritten as:

$$\left(^{26}Mg/^{24}Mg\right)_{\Delta t} = \left(^{26}Mg/^{24}Mg\right)_0 + \left(^{26}Al/^{27}Al\right)_0 \left(^{27}Al/^{24}Mg\right)_m e^{-\lambda \Delta t} \quad (7)$$

Plotting the two measurable parameters of this equation ($^{27}Al/^{24}Mg$, $^{26}Mg/^{24}Mg$) for two or more samples will produce a line whose slope gives not the age, but the $(^{26}Al/^{27}Al)$ at the time when the samples formed (Figure 1b). The time interval between the reference time and the time of sample formation is then:

$$\Delta t = -\left(\ln\left[\left(^{26}Al/^{27}Al\right)_{\Delta t} \Big/ \left(^{26}Al/^{27}Al\right)_0\right]\right)/\lambda \quad (8)$$

To convert these relative ages into absolute ages requires cross-calibration with a chronometer that provides absolute ages. For example, a certain type of mineral inclusion within the Allende meteorite provided a Pb–Pb age of 4567.6 ± 0.4 Ma and an Al-Mg isochron whose slope corresponds to $^{26}Al/^{27}Al = 4.96\ (\pm\ 0.25) \times 10^{-5}$ (Jacobsen et al., 2008). This provides a "pinning point" for the $^{26}Al/^{27}Al$ ratio present in the solar system at a known time. Thus, if analyses of some other sample produced an Al–Mg isochron whose slope corresponded to, for example, $^{26}Al/^{27}Al = 2.5 \times 10^{-5}$, this sample would be one half-life of ^{26}Al, or 750,000 years, younger than the other. Extinct radioactive dating systems thus provide not absolute, but relative, ages. If these relative ages are anchored to an absolute age, as done in the example above, then the extinct system can be used to indicate that the hypothetical sample mentioned above is 4566.8 million years old. A good example of the use of extinct radionuclides is the attempt to date the oldest volcanism in the solar system. Several types of meteorites are interpreted to be lavas produced on small planetesimals. One of these, the D'Orbigny meteorite, has provided Al–Mg, Mn–Cr, Hf–W, and Pb–Pb ages of 4562.8 ± 0.5 Ma, 4564.0 ± 0.6 Ma, 4562.8 ± 1.5 Ma, and 4564.42 ± 0.12 Ma, respectively. These results offer the promise of temporal precisions of 0.002% for the earliest events in solar system history.

The application of radiometric dating

The relatively simple equations given in the previous section provide the basis by which measurements of radioactive decay products can be translated into absolute ages. Applying these chronometers to natural processes requires matching the distinct properties of the many radioactive systems listed in Table 1 to the problem being investigated. Systems with short half-lives can be used to determine precise ages of geologic events only a few to a few thousand years old. Many of these short-lived nuclides are created either in the atmosphere or upper meter of Earth's surface, which makes them particularly amenable to dating a variety of near-surface processes. The concentrations of ^{10}Be or ^{26}Al in quartz in rocks or sediments can be used to date the time when the rock was exposed to cosmic rays, which can provide information on both uplift and erosion rates (von Blanckenburg, 2005) (see *Paleoseismology*). The rates of water movement from surface through subsurface aquifers can be traced with a number of radiometric chronometers (Bethke and Johnson, 2008). The presence of ^{10}Be in the lavas erupted at convergent margins tracks the subduction of surficial sediments to the 100 km + depths of magma generation (Morris, 1991) (see *Subduction Zones*). Carbon-14 is used to date a huge variety of events from the eruption of young volcanoes, movement along faults (see *Earthquakes and Crustal Deformation*; *Archaeoseismology*; *Paleoseismology*), the rates of ocean water circulation and ocean uptake of atmospheric CO_2, and the death of a living organism with its applications in archeology and paleoecology (Broecker, 2005). The longer-lived radionuclides can be applied to a wide variety of issues concerning the evolution of the solid earth, from dating the formation of crustal rocks (see also *Paleomagnetism, Magnetostratigraphy*), to determining the time of continental assembly and breakup (see *Continental Drift*; *Plates and Paleoreconstructions*), to defining the age of the Earth.

The key point in the application and proper interpretation of radiometric dating is understanding exactly what

event is being dated. What "starts" a radiometric clock is some event that changes the composition of a sample and fixes this new compositional state until the sample is dated in the laboratory. For example, ^{14}C often is used to determine the age of young volcanic eruptions. This system works in this application not by dating the rock itself, but by dating charcoal formed when the lava flowed over, and burnt, a bush or tree. What the ^{14}C age actually dates is the time when the plant stopped exchanging carbon with Earth's atmosphere. In most cases, this happened because the plant was killed by the volcanic eruption, in which case, the ^{14}C age accurately dates the eruption. However, if a 100-year-old lava flow were to flow over a 10,000-year-old bristlecone pine tree trunk lying long dead on the ground, the ^{14}C date of the charcoal would be 10,000 years, not 100 years.

The precision of a radiometric age depends on the amount radioactive decay has changed the isotopic composition of the parent or daughter element. This depends primarily on the time passed relative to the half-life of the system, and in systems where measurement of the daughter element is involved, on the degree to which parent and daughter element are fractionated from one another. Thus, one would use ^{14}C with its 5,730 year half-life to date an organic remain from ancient Rome, but it would be useless to date a million year old limestone because the ^{14}C "clock" stopped measuring time when the ^{14}C decayed away after a few half-lives into the history of the limestone. Similarly, ^{147}Sm, with a 106 billion year half-life, is used to date a variety of materials ranging in age from millions to billions of years old, but would be useless to date very young processes because only 7×10^{-15} g of ^{143}Nd is produced every thousand years per ppm of Sm, and this amount simply is too small to measure accurately.

Besides choosing the proper radiometric system for the application, understanding whether a radiometric age is providing an accurate age for the event of interest demands an understanding of the processes that set, and reset, a radiometric clock. For Equation 5 to provide an accurate age demands that the samples used to construct the isochron: (1) all formed at exactly the same time, (2) all had exactly the same initial daughter isotope composition, (3) experienced no change in parent/daughter element ratio between formation of the sample and its measurement in the laboratory, and (4) nothing other than the decay of the parent modified the daughter isotopic composition. In nature, all of these requirements have the potential to fail, but, in some cases, these "failures" can still provide useful information.

A good candidate to meet the requirements above is a volcanic rock. Under conditions ideal for an accurate age, a well-mixed magma will crystallize, over a short time interval after eruption, a variety of minerals with different parent/daughter elemental ratios, but the same initial daughter isotopic composition that they inherit from the magma. Over time, if the minerals experience no chemical exchange with their surroundings, the radioactive decay products will build up allowing their measurement to provide the accurate age of eruption of this volcanic rock. The Apollo 15 basalt 15386 provides evidence that when these criteria are met, ages from many radioactive systems can agree. For this sample, the age (in billions of years) obtained from different radiometric systems are: K-Ar 3.89 ± 0.04, Rb-Sr 3.88 ± 0.01, Sm-Nd 3.85 ± 0.08, and the U–Pb age for zircon from a compositionally similar rock is 3.89.

For volcanic rocks this old, the assumption that the minerals all formed at the same time, at least relative to the ancient age of the rock, likely will be accurate. When one moves to younger volcanic systems, and the use of chronometers with better temporal resolution, the issue of the duration of crystallization becomes important. Several cases have now been presented where different minerals in the same volcanic rock give ages that range from the age of eruption to significantly older. One example is the Coso Volcanic field in California where zircons in one of the rhyolites range in age from the same as a K-Ar date on sanidine from the rhyolite, interpreted as the eruption age, to as much as 200,000 years older (Miller and Wooden, 2004). This result suggests that emplacement and crystallization of distinct magma batches in the crustal magma chamber that eventually fed this eruption is a prolonged process occurring over many thousands of years. Similar results have now been reported in many young volcanic rocks (Cooper and Reid, 2008). Although the age range of the minerals mentioned above is interpreted as reflecting a prolonged magmatic event, another way that an old crystal can get into a young magma is if a crystal from an older rock underlying the volcano is picked up by the magma during its ascent. Finding such "xenocrystic" material, particularly within more viscous, lower melting temperature, silica-rich magmas, is so common that it can be used to detect and even determine the age of older crust buried beneath a volcano, in some cases enabling the identification of older basement where none was previously known to exist (Smyth et al., 2007).

This brings up what is possibly the most insidious cause of an inaccurate radiometric age: the generally poorly-known temperature history of the sample. Because the rate of chemical diffusion within solids increases with temperature, elevated temperatures facilitate chemical changes. Heating a mineral can cause gases, such as He and Ar that are present in a crystal lattice as a result of their production through radioactive decay, to diffuse out of the crystal and escape along grain boundaries. At a temperature of 1,000°C, diffusion will cause a Sr atom in a mineral to move about 2 mm in a million years. If a small grain of a high Rb/Sr ratio mineral, such as mica, is next to a grain of a low Rb/Sr ratio, and high Sr content, mineral like plagioclase, the ingrowth of radiogenic ^{87}Sr in the mica will be diluted by diffusional exchange with the unradiogenic Sr in the plagioclase. Diffusion thus makes all radioactive chronometers "thermochronometers" that date the time when the material of interest reached a low-enough temperature to stop diffusional resetting of

the radiogenic ingrowth. Because rates of diffusion are a function both of the element that is diffusing and the structure of the crystal through which it is diffusing, different radiometric systems, and different minerals, can have different sensitivities to temperature excursions. This gives rise to the concept of "closure" or "blocking" temperature, above which the diffusion rate is too high to allow for the buildup of the radioactive decay product. In other words, the radiometric clock does not start until the mineral falls below its closure temperature. In the Coso example above, the K–Ar age obtained for the sanidine is interpreted as the eruption age because even if this mineral formed well prior to eruption, the 200–400°C closure temperature of the K–Ar system in sanidine (Figure 2) is so low that the radiogenic ^{40}Ar being produced in the sanidine was diffusing out as fast as it was being produced because of magma temperatures in the range of ~750°C.

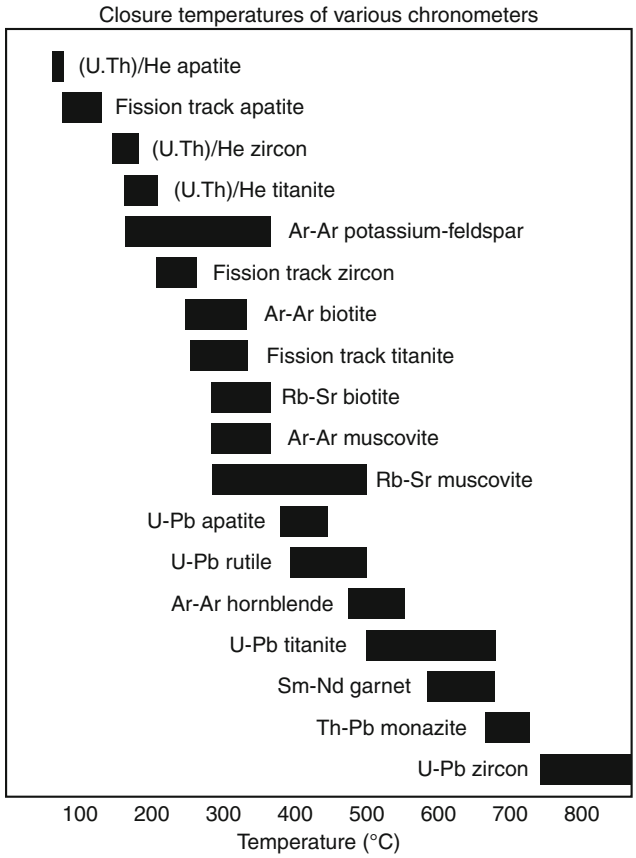

Absolute Age Determinations: Radiometric, Figure 2 Closure temperatures for various radiometric systems in different minerals. The fission track technique counts the density of damage tracks made in crystals due to the fission of ^{238}U. Coupled with the measurement of U concentration in the crystal, the density of fission tracks can be converted into a radiometric age. Figure modified from (Pollard, 2002 – http://pangea.stanford.edu/~dpollard/NSF/main.html) which was adapted from a figure produced by P. Fitzgerald, S. Baldwin, G. Gehrels, P. Reiners, and M. Ducea.

In contrast, the closure temperature of the U–Pb system in zircon is higher than the magma temperature, so as soon as the zircon first crystallized, its U–Pb clock started to record time. Temperature-induced diffusional resetting of radiometric systems may make interpretations of ages a bit more difficult, but it creates a new field – thermochronometry – that constructs time-temperature histories for various geologic processes (Reiners and Ehlers, 2005). Though many radiometric systems can be used for thermochronometry, the oldest radiometric dating technique, the decay of U and Th to He, has been reenergized (Farley, 2002) because the low closure temperature of the U,Th – He system can be used to address geological processes such as the rate of mountain uplift or surface erosion by telling the time when a rock arrived close enough to Earth's surface to cool below the closure temperature of the radiometric clock (Reiners and Brandon, 2006).

While the appreciation and use of thermochronometry has been the primary growth field in radiometric geochronology in the last decade, other efforts are directed at finding ways to avoid reset ages. The traditional way to do this is to move to sample sizes much larger than diffusion lengths. This is the basis for "whole rock isochrons" where kilogram rock samples are homogenized and measured as an individual point on an isochron. Although this approach has produced some accurate ages, it suffers two main weaknesses. First, deciding whether all the rocks included on an isochron are the same age is not always easy, particularly for ancient, highly deformed, gneisses where this approach often is applied. Second, in order to obtain a sufficient range in parent/daughter ratio to precisely determine an isochron, compositionally distinct rocks are usually included on the isochron. Judging from modern igneous rocks, large compositional distinctions often are associated with variable initial isotope composition, which would violate the requirement that all the samples used to construct an isochron have the same initial isotope composition. Where whole rock isochrons can be useful is in detecting when much older components are involved in the genesis of younger rocks. A good example of this are the Sm-Nd data for lunar basalts where mineral isochrons of individual samples provide eruption ages generally less than 4 billion years, but the whole rock data scatter about a line corresponding to an age near 4.45 Ga (Carlson and Boyet, 2009). The precision of this older age is debatable, as is its interpretation, but it could imply that the younger basalts are made by melting source materials in the lunar interior that formed from some global differentiation event on the Moon that occurred some time near 4.45 Ga. Memory of this event was erased from the minerals in the basalts, that know only of their crystallization from the magma, but the magmas themselves may "remember" the events that led to the formation of their source materials in the lunar interior.

The other approach to avoiding thermally reset ages is to use minerals whose crystal structure allows only very slow diffusion. One curious example is diamond.

Diamond cannot be dated directly because it contains insufficient amounts of the radioactive elements, but it often contains as inclusions minerals that can be dated. Even though these minerals were formed, and have been stored, at temperatures above 1,000°C and depths greater than 150 km in the mantle (see *Lithosphere, Continental: Thermal Structure*), the encapsulation by the diamond does not allow them to communicate through diffusion with their surroundings. As a result, dating of inclusions in diamond show that diamond formation in the mantle has occurred over a good part of Earth history, with the oldest diamonds being approximately 3.5 Ga (Pearson and Shirey, 1999) (see *Lithosphere, Continental*).

By far, the most commonly used and most versatile way to avoid reset ages is with the application of the U–Pb system in zircon (Hanchar and Hoskins, 2003). The strengths of U–Pb zircon dating include: (a) very high U–Pb closure temperature, (b) resistance to chemical modification through alteration and metamorphism, (c) high U concentrations, but initially vanishingly small Pb contents, (d) the U–Pb system includes two independent decay schemes that allow tests to determine whether or not the age has been disturbed (Wetherill, 1956), (e) among the long-lived radioisotopes, the relatively short half-life of ^{235}U allows highly precise ages to be obtained for ancient rocks, (f) both the trace element concentrations and Hf isotope composition in zircon provide information on the nature of the source rock from which the zircon was derived, and (g) U–Pb ages can be obtained in samples as small as fragments of individual grains or even spots, tens of microns in diameter, ablated with either lasers or ion beams. Perhaps the only weakness of zircon is that it is not found in all rock types, occurring primarily in felsic igneous rocks. These characteristics explain the many varied applications of zircon U–Pb dating that include the discovery of the oldest dated material on Earth, 4.36 Ga zircons from quartzites in western Australia (Wilde et al., 2001), to high-precision calibration of the geologic timescale (Bowring and Schmitz, 2003), to the previously described use of zircons to determine the duration of crystallization in the magma chambers of young volcanic rocks.

Summary and conclusions

Continually improving analytical capabilities coupled with expanding appreciation of the physical controls on what sets, and resets, radiometric clocks are allowing ever-increasing expansion of this now century-old approach. The variety of radioactive species now in use provide the ability to determine absolute ages for geologic processes that occur over timescales that range from days to the age of the Earth and solar system.

Bibliography

Bard, E., and Frank, M., 2006. Climate change or solar variability: What's new under the sun? *Earth and Planetary Science Letters*, **248**, 1–14.

Bethke, C. M., and Johnson, T. M., 2008. Groundwater age and groundwater age dating. *Annual Review of Earth and Planetary Sciences*, **36**, 121–152.

Bowring, S. A., and Schmitz, M. D., 2003. High-precision U-Pb zircon geochronology and the statigraphic record. *Reviews in Mineralogy and Geochemistry*, **53**, 305–326.

Boyet, M., Carlson, R. W., and Horan, M., 2010. Old Sm-Nd ages for cumulate eucrites and redetermination of the solar system initial ^{146}Sm/^{144}Nd ratio. *Earth and Planetary Science Letters*, **291**, 172–181.

Broecker, W. S., 2005. Radiocarbon. In Keeling, R. K. (ed.), *Treatise on Geochemistry*. Amsterdam: Elsevier, pp. 1–18.

Carlson, R. W., and Boyet, M., 2009. Short-lived radionuclides as monitors of early crust-mantle differentiation on the terrestrial planets. *Earth and Planetary Science Letters*, **279**, 147–156.

Cooper, K. M., and Reid, M. R., 2008. Uranium-series crystal ages. *Reviews in Mineralogy and Geochemistry*, **69**, 479–544.

Dickin, A. P., 2005. *Radiogenic Isotope Geology*, 2nd edn. Cambridge: Cambridge University Press.

Fairbanks, R. G., Mortlock, R. A., Chiu, T.-Z., Cao, L., Kaplan, A., Guilderson, T. P., Fairbanks, T. W., Bloom, A. L., Grootes, P. M., and Nadeau, M.-J., 2005. Radiocarbon calibration curve spanning 0–50, 000 years BP based on paired 230Th/234U/238U and 14C dates on pristine corals. *Quaternary Science Reviews*, **24**, 1781–1796.

Farley, K. A., 2002. (U-Th)/He dating: techniques, calibrations, and applications. In Porcelli, D., Ballentine, C. J., and Wieler, R. (eds.), *Reviews in Mineralogy and Geochemistry*: Noble gases in geochemistry and cosmochemistry, pp. 819–844.

Faure, G., and Mensing, T. M., 2005. *Isotopes: Principles and Applications*, 3rd edn. Hoboken: John Wiley & Sons.

Friedrich, M., Kromer, B., Spurk, M., Hofmann, J., and Kaiser, K. F., 1999. Paleo-environment and radiocarbon calibration as derived from Late Glacial/Early Holocene tree-ring chronologies. *Quaternary International*, **61**, 27–39.

Hanchar, J. M., and Hoskins, P. W. O., 2003. Zircon, *Reviews of Mineralogy and Geochemistry*, **53**, 500.

Holmes, A., 1913. *The Age of the Earth*. London: Harper and Brothers.

Jacobsen, B., Yin, Q., Moynier, F., Amelin, Y., Krot, A. N., Nagashima, K., Hutcheon, I. D., and Palme, H., 2008. ^{26}Al-^{26}Mg and ^{207}Pb-^{206}Pb systematics of Allende CAIs: canonical solar initial ^{26}Al/^{27}Al reinstated. *Earth and Planetary Science Letters*, **272**, 353–364.

Miller, J. S., and Wooden, J. L., 2004. Residence, resorption and recycling of zircons in Devils Kitchen rhyolite, Coso Volcanic field, California. *Journal of Petrology*, **45**, 2155–2170.

Morris, J. D., 1991. Applications of cosmogenic ^{10}Be to problems in the Earth sciences. *Annual Review of Earth and Planetary Sciences*, **19**, 313–350.

Pearson, D. G., and Shirey, S. B., 1999. Isotopic dating of diamonds. In Lambert, D. D., and Ruiz, J. (eds.), *Application of Radiogenic Isotopes to Ore Deposit Research and Exploration*. Boulder: Society of Economic Geologists, pp. 143–172.

Reiners, P. W., and Ehlers, T. A., 2005. Low-temperature thermochronology: Techniques, interpretation, and applications, *Reviews in Mineralogy & Geochemistry*, **58**, 622.

Reiners, P. W., and Brandon, M. T., 2006. Using thermochronology to understand orogenic erosion. *Annual Review of Earth and Planetary Sciences*, **34**, 419–466.

Rutherford, E., 1906. *Radioactive Transformations*. New York: Scribner's.

Smyth, H. R., Hamilton, P. J., Hall, R., and Kinny, P. D., 2007. The deep crust beneath island arcs: inherited zircons reveal a Gondwana continental fragment beneath East Java, Indonesia. *Earth and Planetary Science Letters*, **258**, 269–282.

Truran, J. W. J., and Heger, A., 2005. Origin of the elements. In Davis, A. M. (ed.), *Treatise on Geochemistry*. Amsterdam: Elsevier, pp. 1–16.
von Blanckenburg, F., 2005. The control mechanisms of erosion and weathering at basin scale from cosmogenic nuclides in river sediments. *Earth and Planetary Science Letters*, **237**, 462–479.
Wetherill, G. W., 1956. Discordant U-Pb ages. 1. *Transactions on American Geophysical Union*, **37**, 320–326.
Wilde, S. A., Valley, J. W., Peck, W. H., and Graham, C. M., 2001. Evidence from detrital zircons for the existence of continental crust and oceans on Earth 4.4 Gyr ago. *Nature*, **409**, 175–178.

Cross-references

Archaeoseismology
Continental Drift
Continental Rifts
Energy Budget of the Earth
Geodynamics
Lithosphere, Continental
Lithosphere, Continental: Thermal Structure
Paleomagnetic Field Intensity
Paleomagnetism, Magnetostratigraphy
Paleoseismology
Plate Tectonics, Precambrian
Radiogenic Heat Production of Rocks
Subduction Zones

ARCHAEOMAGNETISM

Donald H. Tarling
School of Earth, Ocean and Environmental Sciences, University of Plymouth, Plymouth, UK

Synonyms

Magnetic dating, archaeological; Remanence dating

Definition

Archaeomagnetism is the study of all remanent magnetization associated with materials found in, or associated with, an archaeological context. In practice, it is the application of paleomagnetic techniques to archaeological materials, predominantly in terms of their uses in dating or "sourcing" such materials. This generally means that magnetic surveys are not usually considered "archaeomagnetic," other than when used to provide information on the actual directions and intensities of the remanent magnetizations of the materials causing the anomalies.

As most applications of archaeomagnetic studies relate to magnetic dating, these aspects are described first.

Basic features

Most materials within archaeomagnetic contexts contain iron oxide minerals that are capable of carrying a magnetic remanence acquired at some past time. More rarely, iron sulphides and hydroxides can carry such remanences. Even more rarely, a remanence can be carried by pure iron, nickel and cobalt and their alloys, and in very specific conditions, iron sulphates. The commonness of magnetite (Fe_3O_4) and hematite (Fe_2O_3) makes these almost always the dominant minerals involved. Such ferromagnetic (*sensu lato*) minerals can acquire a *thermal remanence* in the Earth's magnetic field (or of nearby magnetic objects) while cooling from higher than ambient temperatures, *chemical remanences* as a result of crystalline or compositional changes. Some archaeological materials can comprise iron objects, but these are generally poor recorders of early remanences, being generally magnetically "soft." All archaeological materials can become comminuted and eventually deposited as sediments (*v.i.* Archaeological sediments) in which the individual magnetic grains can be magnetically aligned during their deposition in aqueous or aeolian conditions, resulting in a *detrital magnetization* (see *Paleomagnetism, Principles* for details).

In an archaeological environment, it is unlikely that only one form of remanence is present. It can also be presumed that some of the originally acquired remanence will have decayed with time, and other time-dependent magnetizations, *viscous magnetizations*, will have been acquired as the materials lay within a geomagnetic field that gradually changes in both direction and intensity. In order to determine the direction and intensity of the geomagnetic field for some specific time in the past (such as when last heated or deposited), it is necessary to remove such viscous magnetization. Where such viscous magnetizations are not associated with chemical changes, they can be removed by partial demagnetization in alternating magnetic fields or heating in zero-magnetic field in nonmagnetic furnaces. Alternating field demagnetization randomizes the low coercivity components of remanence, that is, the viscous remanences, leaving the high coercivity components unchanged. Partial thermal demagnetization reduces the relaxation time of all contained minerals, that is, the time taken for the direction of individual grain magnetization to relax into the ambient field direction. As the ambient field is zero, the grains with low relaxation times (those that carry the viscous magnetizations) thereby become randomized, leaving the high relaxation grains still in original directions. (For further detail, see *Paleomagnetism, Principles*.) Such partial demagnetization procedures are necessary for magnetic dating using directions or intensity. Statistical analyses, initially Principle Component Analyses, are then made to determine the number, direction, intensity, and precision of the magnetic vectors present in any single sample (see *Paleomagnetism, Measurement Techniques and Instrumentation* for details). The isolated individual sample vectors defined within some 5° that are considered to have been acquired originally are then combined, usually using Fisherian Statistics and giving equal weight to each sample vector, to provide a mean site direction. (Where individual oriented hand samples have been subsampled, these subsamples are combined to obtain the sample values that then yield the site mean value.)

Such treatments normally require different instrumentation for dating based on directions than those for dating based on intensity and are described separately. The theoretical bases are the same.

Archaeological site sampling

Directional analyses

Generally between 7 and 20 individually oriented samples are taken. This enables orientation errors to be averaged, as well as measurement errors. Ideally such samples are distributed evenly throughout the structure being sampled, although concentration is made on materials that are most likely to yield meaningful results and where the physical stability (since acquiring remanence) is better established. Sample orientation in situ is preferably undertaken nonmagnetically (sun compass, gyro-theodolite, or by sightings) as the objects themselves commonly distort magnetic compass readings. It is also desirable that the nature and conditions at the site, with the in situ samples, is recorded so that, when completing the analyses, possible causes from anomalous determinations can be better evaluated (see *Paleomagnetism, Measurement Techniques and Instrumentation*).

Paleo-intensity analyses

Samples for such studies do not need to be oriented while in situ nor need the samples be still in their original positions in which their remanence was acquired. However, such orientations can be useful is assisting assessments of samples that show more than one remanent magnetic vector. Generally, some three to five samples are selected for study from any one archaeological site (see *Paleomagnetic Field Intensity*).

Magnetic dating based on the direction of remanence

This dating method depends on the longtime spatial variations ($>\sim$10 years) of the geomagnetic field (see *Geomagnetic Field, Secular Variation*). Analyses of the present-day geomagnetic variations suggest that, at a medium latitude location, the observed geomagnetic field in a circular area of some 550 km radius ($\sim$1 Mkm^2) can be modeled as that of a geocentric inclined dipole field within an error of $\sim$0.5° (solid angle) in direction. At greater distances, the error increases to $>$1° (solid angle) rendering the model increasingly unreliable for comparing the directions of remanence at more distant sites. Such modeling enables "Master Curves" (Paleo-Secular Variation Curves) of directional change to be constructed using previously studied sites for specific regions, usually for a specific country or groups of small countries. In the UK, most English and Welsh observations were corrected to a central location, Meriden, while French observations were generally corrected to Paris.

Master Curves are now more commonly calculated within a far more sophisticated statistical modeling, notably hierarchical Bayesian modeling (Lanos et al., 2005). In such analyses, the Gaussian errors for the date assignments as well as for directional properties are incorporated in the construction of the Master Curves. Such Bayesian statistics similarly incorporate harmonic analyses. Spherical Cap analyses have the objective to determine the geomagnetic field variations attributable to fields at the Earth's core (Pavón-Carrasco et al., 2008). The latter method is therefore more appropriate for geomagnetic field modeling (see *Geomagnetic Field, Theory*).

Relative dating

Nearby sites (within some 50–80 km) that acquired their remanence at the same time will exhibit identical (within 1°) directions of remanence. Consequently, nearby sites with differing directions of remanence can be considered to have acquired their remanence at different times. Conversely, similar directions can indicate similar ages for their remanence acquisition. However, identical geomagnetic directions can occur in the same location at different times. When such repeat directions occur at time intervals of a few 100 years, the archaeological context is often adequate to distinguish between alternative age assignments.

Chronological dating

This dating method is dependent on the secular variation of the geomagnetic field being known for the region being investigated (see *Geomagnetic Field, Secular Variation*). As the current geomagnetic theories for the origin of the geomagnetic field are still evolving (see *Geomagnetic Field, Theory*), this usually requires previously well-dated (by non-archaeomagnetic means) site values to be available. In newly studied areas, the method is clearly inhibited by the lack of such data, but as more and more observations are obtained, the past directions of the geomagnetic field become increasingly well defined. Archaeomagnetic dating is thus an unusual scientific dating technique as its precision increases as more observations accumulate.

Magnetic polarity and polarity excursion dating

This dating application is based on unusual aspects of the long-term geomagnetic behavior. On scales of a few thousand years, the geomagnetic field can undertake major excursions away from its normal direction, geomagnetic events, or excursions. On timescales of a few 100,000 years, the Earth's magnetic field changes polarity – the North magnetic pole becoming the South magnetic pole, and vice versa for the South magnetic pole. Consequently, some geomagnetic excursions occur on archaeological timescales, and the younger polarity changes occur on archaeological-anthropological timescales (see *Geomagnetic Excursions*; and *Geomagnetic Field, Polarity Reversals* for more detailed considerations).

Magnetic dating based on the intensity of remanence

Relative dating can be based on the determination of paleo-intensities of the ancient field in a similar way as for direction (qv). Most current studies are directed toward defining the changes in geomagnetic intensity during archaeological time although sufficient quantities of high quality paleo-intensity determinations are now becoming

available for specific regions, enabling chronological dating to be undertaken. As for directional studies, when past records of the Earth's magnetic field intensity are available, a Master Curve can be constructed for a similar circular area of ~1 Mkm^2, radius of ~550 km, as for directional studies.

Errors

General errors

These apply to both directional and intensity dating techniques.

1. It is usually assumed that any effects of weathering and other environmental changes are minimal and that the magnetic grains carrying the remanence of interest are essentially unaffected. However, some weathering products, such as goethite and hematite, can carry high-stability remanence. It is desirable that, as far as practicable, unweathered materials are collected.
2. During partial demagnetization, it is assumed that no chemical or structural alterations occur to the existing magnetic minerals and that no new magnetic minerals are formed. Such changes are far more likely during thermal demagnetization than by alternating magnetic field techniques and are usually monitored by repeated measurements of the initial susceptibility. This is, however, a coarse measure and magnetic domain changes (see *Magnetic Domains*) which can occur with no clear change in susceptibility.
3. Both directions and intensities can be affected by magnetic anisotropy (shape and crystalline) that may be associated with the sample shape, the shape of contained minerals and the orientations of their crystallographic axes (see *Magnetic Anisotropy*).
4. Lightning strikes at times subsequent to the original acquisition of remanence, and have electromagnetic effects that can drastically alter the magnetic remanence. Although mostly associated with electrical charges that usually travel through surface waters, these effects can penetrate. Such effects can usually be recognized by their high intensities and tendency to be in random directions.
5. The local geomagnetic field direction and intensity may well be distorted if there were nearby magnetized objects, natural or manufactured, at the time of remanence acquisition.
6. The behavior of the geomagnetic field is still poorly defined and, particularly at high magnetic latitudes, can show major diurnal variations. It also appears that secular variations are not necessarily smooth, but may occur in "jerks" (see *Geomagnetic Field, Secular Variation*) although these appear to be mostly within the current experimental error of the technique.
7. The geomagnetic field over time can return to previous direction and intensity values. When such "crossover" points occur in the Master Curves at sufficiently different times, then the archaeological age constraints on the site may enable the most likely chronological age to be applied. However, most extant Master Curves are likely to still be distorted by some studies for which the archaeological or chronological age has subsequently been modified. However, such "anomalous" sites becoming increasingly recognized as databases increase.

Errors specific to directional dating

In addition to the general errors, directional studies are sensitive to the oriented samples having remained in situ since they acquired their remanences. In a solid structure, such loose materials can be readily identified, but individual parts of some structures can have undergone motions relative to the rest of the structure, for example, kiln-wall "fall-out" or "fall-in." On hillside, it is also possible that the whole structure may have undergone motion away from where the remanence was acquired. Thus, a knowledge of the archaeological controls on possible motions of the site is essential.

Errors specific to intensity dating

In addition to the general errors, paleo-intensity studies are sensitive to the "cooling rate" of the acquired magnetic properties. The naturally acquired remanence will commonly have been acquired over times that can be of the order of several days, while the laboratory studies are necessarily on far shorter times scales. The laboratory redox conditions during cooling are normally very different.

Overall error assessment

While there are many potential sources of error in archaeomagnetic dating, in most archaeological sites where the conditions are clear and the materials largely pristine, the errors arising appear to be only rarely of sufficient magnitude to warrant rejection.

Specialized applications

Murals and plaster

Remarkably, it has been shown that pigments can carry a remanence relating to the time when they were applied. Where such pigments have been applied to walls, their remanence has been shown to relate to the time that the pigments were applied, particularly in tempera paintings – either originally or during subsequent retouching. It seems most likely that this remanence is associated with hematite and was acquired "detritally," that is, by rotation of the grains while still fluidized (Lanza et al., 2009). Similar observations have also been shown for plaster work (Soler-Arechalde et al., 2006).

Object reconstruction

Specific artifacts, such as pottery, when fired, obtain a uniform magnetization in the ambient geomagnetic field as they cool within the furnace. If broken, individual shards retain this original remanence and can be reassembled to assist in defining the original shape of the pot (Burnham and Tarling, 1975).

Archaeological sediments

As sediments are deposited within an archaeological site, any contained already magnetized grains are influenced by the ambient geomagnetic field. As these alignment forces are weak (compared with the effects of gravity and flow motions) only a percentage of the magnetic grains are aligned and such alignments can be gravitational flattening during the deposition process. However, the more magnetically stable grains (usually with single-domain dimensions of ~1 μm) can rotate into full alignment while they are still fluidized immediately after deposition. However, such alignments can be modified by meniscus forces as the water table subsequently rises or falls. Sedimentary minerals also undergo a series of chemical reactions as they adjust to their new environment. Consequently, it is often difficult to establish the true direction of the geomagnetic field at the time of deposition with sufficient certainty to assign ages based on the magnetic determinations. However, there are archaeological sites, such as basal sediments, deposited immediately after a ditch had been cut, that appear to be recording the geomagnetic field direction at that time.

Magnetic "sourcing"

Magnetic sourcing attributes an object to a particular location on the basis of its magnetic properties. For example, an obsidian arrowhead can sometimes be sourced to the obsidian outcrop from which it was originally fashioned.

The physical basis for this is that the compositions and grains sizes of the magnetic minerals within a rock can be specific to a particular outcrop. Each outcrop also tends to have a slightly different cooling history and became magnetized by a specific geomagnetic field strength. Several magnetic properties can be rapidly and cheaply measured, such as its initial (low field) susceptibility, its saturation remanence, and its intensity of natural remanence, are sufficient to identify a specific outcrop. Generally, the range of magnetic properties in most sedimentary rocks is too great to allow such assignments, but obsidians, rapidly cooled volcanic glasses, commonly have a range of magnetic properties that are either unique to that outcrop or to only two or three outcrops.

Summary

The study of the magnetic properties of archaeological materials, archaeomagnetism, is particularly significant in geophysics as it enables secular variations in the direction and strength of the geomagnetic field over timesscale that are far longer than those for direct measurement (~400 years). In comparable magnetic studies of rocks, paleomagnetism, these secular variations are commonly averaged out during the processes by which rocks acquire their remanent magnetization. Conversely, archaeomagnetic records provide an additional dating tool for archaeologists. As a comparative dating tool, archaeomagnetism enables relative dating between nearby samples (100–200 km) within ~10–20 years. As a dating tool, it is mainly dependent on the validity of the ages used to compile the regional Master Curve. It is thus unique, as a scientific dating method, in that as more data are acquired, age "outliers" can be identified and their age reassessed. Consequently, the Master Curves are continually improving and, ultimately, could have the same precision as for relative dating. There are also interesting applications in using such observations in conservation studies and establishing past environmental conditions.

Bibliography

Batt, C. M., and Zanarini, I. (eds.), 2008. Archaeomagnetic applications for the rescue of cultural heritage (AARCH). *Physics and Chemistry of the Earth*, **33**(6–7), 403–608.

Burnham, R. J. P., and Tarling, D. H., 1975. Magnetisation of shards as an assistance to the reconstruction of pottery vessels. *Studies in Conservation*, **20**, 152–158.

Lanos, Ph., Le Goff, M., Kovacheva, M., and Schnepp, E., 2005. Hierarchical modeling of archaeomagnetic data and curve estimation by moving average technique. *Geophysical Journal International*, **160**, 440–476.

Lanza, R., Zanella, E., and Sandino, S., 2009. Magnetic remanence of haematite-bearing minerals. *Geophysical Research Letters*, **36**, L24302.

Pavón-Carrasco, F. J., Osete, M. L., Torta, J. M., Gaya-Piqué, L. R., and Lanos, Ph., 2008. Initial SCHA.DI.00 regional archaeomagnetic model for Europe for the last 2000 years. *Physics and Chemistry of the Earth*, **33**(6–7), 597–608.

Soler-Arechalde, A. M., Sánchez, F., Rodriguez, M., Caballero-Miranda, A., Goguitchaichvil, A., Urrutia-Fufugauchi, J., Manzanilla, L., and Tarling, D. H., 2006. Archaeomagnetic investigation of oriented pre-Columbian lime-plasters at Teotihuacan, Mesoamerica. *Earth Planets Space*, **58**, 1433–1439.

Cross-references

Geomagnetic Excursions
Geomagnetic Field, Polarity Reversals
Geomagnetic Field, Secular Variation
Geomagnetic Field, Theory
Magnetic Anisotropy
Magnetic Domains
Paleomagnetic Field Intensity
Paleomagnetism, Measurement Techniques and Instrumentation
Paleomagnetism, Principles

ARCHAEOSEISMOLOGY

Klaus-Günter Hinzen
Earthquake Geology Group, Institute of Geology and Mineralogy, Cologne University, Bergisch Gladbach, Germany

Synonyms

Earthquake archeology

Definition

The study of pre-instrumental earthquakes that, by affecting locations of human occupation and their environments,

have left their mark in ancient structures uncovered by means of archaeological excavations or pertaining to the monumental heritage (Buck and Stewart, 2000; Galadini et al., 2006).

Introduction

Ever since man-made structures have been erected, earthquakes have left their marks on these constructions. However, damages in archaeologically excavated buildings or continuously preserved monuments are often hard to unravel in terms of the causative effects. The use of archaeological data to investigate unknown or poorly known historical earthquakes and descriptions of earthquake effects recorded in the archaeological heritage started in the nineteenth and early twentieth century (e.g., De Rossi, 1874; Schliemann, 1881; Evans, 1928). Since the 1980s, the increased interest in the subject led to the publication of special volumes and articles in seismological and geological journals (e.g., Guidoboni, 1989; Stiros and Jones, 1996; McGuire et al., 2000; Galadini et al., 2006; Reicherter et al., 2009). While earlier investigations were dominated by the qualitative description of damage records, more recent studies take a quantitative approach. The main questions to be answered by archaeoseismic investigations are (1) how probable are seismic ground motions, or secondary earthquake effects, as the cause of damage observed in man-made structures from the past, (2) when did the damaging ground motion occur, and (3) what can be deduced about the nature of the causing earthquake.

Archaeoseismic observations

The marks in ancient structures relevant for archaeoseismology fall into four main categories: (1) displacements along shear planes directly linked to the earthquake fault plane or side branches of it. In particular, earthquakes with a strike slip mechanism can leave distinctive traces in buildings and lifelines such as aqueducts, roads, and sewer systems. Case studies (e.g., Ellenblum et al., 1998; Meghraoui et al., 2003) show that under favorable conditions the amount of slip and in case of repeated events the slip rate of the faults can be revealed. (2) Off-fault-shaking effects including fractured building elements, tilted walls, shift of building elements, lateral warping, breaking and overthrow of walls, rotations of vertically oriented objects (tomb stones, columns, monuments). For most of these features, a seismogenic origin is not the only possible interpretation. Therefore, alternative causes must be taken into account in the damage analysis. (3) The secondary shaking affects lateral spreading and cyclic mobility as a consequence of liquefaction of the subsurface. Liquefaction always requires a certain level of dynamic excitation. So secondary damages in buildings and monuments due to liquefaction help exclude alternative causes from a damage scenario. (4) Archaeologically detected abandonment of a site and evidence of repair and rebuilding. These observations are mainly of interest in connection with the reasons mentioned before because as a single observation in general they do not give enough evidence for the conclusion of a seismogenic cause (Galadini et al., 2006).

While the first category is limited directly to the linear features of active faults, off-fault shaking affects a much larger area and is more common but harder to prove. Ancient structures show deformations related to seismic shaking similar to those observed in recent earthquakes. Typical earthquake effects on masonry walls are (1) cross fissures, due to stress concentrations often nucleating at corners of doors and windows, driven by shear forces, (2) corner expulsion of walls caused by differential movements in orthogonal directions, (3) horizontal and independent lateral and rotational shift of wall blocks, best visible in uncemeted walls made of rectangular blocks, (5) spall of block corners due to stress concentrations, (6) height reduction by vertical crashing, (7) movement of keystones and rupture of arch piers, (8) rotation of vertically oriented objects, (9) domino-like toppling of structured columns and walls. Examples are shown in Figure 1. Following the term seismite, used for seismically disturbed sediment layers, the above-mentioned deformations may be called archaeoseismites. Several of these deformations may also originate without dynamic earthquake excitation. In these cases, a single piece of evidence or at a single edifice only cannot be considered a conclusive archaeoseismite. If damages are identified as archaeoseismites, intensities can be derived following the classical macroseismic methods.

Methods

Archaeoseismology requires the integration of several scientific disciplines. Figure 2 shows a scheme of workflow in a quantitative archaeoseismic study. Besides archaeological and seismological methods, input from geodesy, pure and applied geology, and civil engineering is needed (Ambrasyes, 2006). Physical absolute dating techniques including radiometric methods, luminescence methods, and dendrochronology are necessary to determine a time window for the damaging event. In case of multiple events, the rough dates are crucial for seismicity models and hazard analysis.

The first step in studying field cases is the documentation and analysis of damages to the archaeologically excavated buildings or objects. In addition to the important traditional excavation techniques and classical measurements and drawings, 3D imaging techniques have proved their usefulness in archaeoseismic field cases. Photogrammetry and laserscanning are fast in the field and allow detailed analysis and post processing, especially a quantification of deformations, fractures, etc. In cases where building parts are fragile and cannot be conserved in the original finding situation, successive laser scans during the excavation offer the possibility to build virtual 3D models. In ideal cases, the seismological relevant data can be acquired during an ongoing excavation. Important

Archaeoseismology, Figure 1 Examples of deformations and damages which possibly are earthquake effects: (**a**) Horizontally deformed wall of a crusader fortress build on top of the Dead Sea Transform Fault in the Jordan Valley; (**b**) deformed vault of a Roman sewer in Cologne, Germany; (**c**) toppled columns of a Byzantine church in Sussita located above the Sea of Galilee; (**d**) toppled column of the great palace in Patra, Jordan; (**e**) moved block in an arch of the Nimrod fortress in the Golan Heights; (**f**) shifted blocks of an analemma of a Roman theatre in Pınara, SW Turkey; (**g**) moved blocks of a corner wall of a Roman monument in Patara, SW Turkey; (**h**) shifted blocks of a Roman grave house in Pınara, SW Turkey; (**i**) spall of block corners, same object as in (**g**);(**j**) broken and horizontally displaced fortification wall of the Roman Tolbiacum (Zülpich, Germany); (**k**) rotated Lycien sarcophagus in Pınara, SW Turkey.

is the complete documentation of the stratigraphy of debris layers, which can reveal the decay rate of structures (Galadini et al., 2006). Building collapse may be sudden, progressive, or a combination of both. The progressive deterioration of walls results in accumulations having maximum thickness close to the wall feeding the material. The thickness decreases a short distance from the wall. In case of height reduction of walls or buildings due to earthquake effects, the debris is more distributed. Sometimes even complete walls topple to one side; in this case, the impact pattern can help to constrain ground motion amplitudes. However, if the findings of previous excavations are archaeoseismologically analyzed, the current situation and available excavation reports form the database. Possible alterations of the excavated objects since the first excavation and shortcomings in the documentation, especially if earthquake actions were not considered at the time of the original excavation, might hinder the interpretation.

Depending on site conditions, exploration, and modeling of the properties of the local geology at the site is an important second step. Several of the above-mentioned deformations can also be caused by slow, quasi-static deformations of the subsoil, and ground amplification due to shallow soft sediments can significantly amplify seismic shaking. If the latter is not taken into account, the size of the damaging earthquake can easily be overestimated.

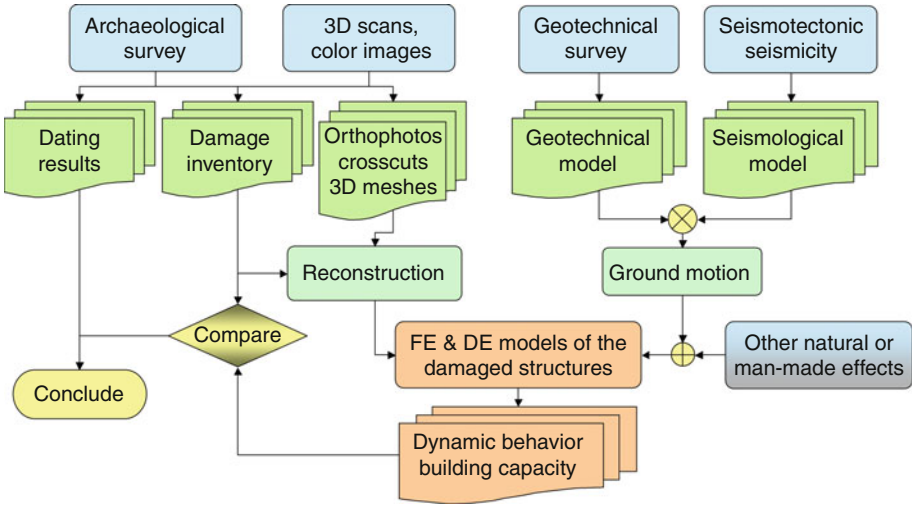

Archaeoseismology, Figure 2 Schematic work flow in a quantitative multidisciplinary archaeoseismic study. The dynamic behavior is studied by finite element (FE) or discrete element (DE) methods.

Only on rare occasions, site-specific strong motion records from recent earthquakes will be available and help to prove or disprove proposed damage scenarios. To overcome this lack of information, the calculation of synthetic seismograms based on models of the capable faults and local geology have been used to better ascertain the probability of a seismogenic cause of the damages and name faults on which the damaging earthquake occurred. When other natural forces (flooding, storm, mass movement) or even human action also come into consideration, their action on the excavated objects has to be tested as well.

Reconstructions of the damaged archaeological objects are the basis for determining the dynamic behavior and the vulnerability of the ancient buildings. Common earthquake engineering techniques including finite element and discrete element modeling are used to analyze the reaction of the buildings to the estimated seismic loading functions. Results from such models are compared to the damages observed in situ.

The most challenging task of an archaeoseismic study is the determination of source parameters of the earthquake which caused the analyzed damages. While timing of the earthquake has to be done by archaeological techniques, including classical archaeological stratigraphy and the above-mentioned physical dating, location and strength of the earthquake can only by narrowed down with seismological models. A territorial approach (Galadini et al., 2006), in which the collected information from the surroundings of an archaeological site are taken into account, is the most promising tool to determine earthquake source parameters.

Summary

In the past decades archaeoseismology has evolved as a new branch of seismological sciences. While palaeoseismology focuses on the marks left by earthquakes in the geological record, archaeoseismologists analyze and interpret marks in the archaeological record and in preserved monuments.

The use of quantitative methods in archaeoseismology, including calculation of synthetic site-specific strong motion seismograms, modeling of natural non-earthquake-related forces, anthropogenic forces, and finite or discrete element models of structures, supports conclusive discrimination between potential damage scenarios. However, if model parameters cannot be well constrained, modeling result uncertainties might still be too large to draw definite conclusions. Common sense interpretations of archaeoseismites as solitary evidence are generally too vague to complement earthquake catalogs for a seismic hazard analysis. Recent advances in ground motion simulation methods and computational possibilities promise to refine quantitative archaeoseismological methods and establish them at levels equal to historical and palaeoseismologial methods. Finally, even if an archaeoseismic study does not deliver the often-requested improvement of hazard determination, it can still advance our picture of the past by attempting to answer open archaeological, historical, and geologic questions in a scientific manner. And following Ambrasyes (2006): "Surveying and mapping an archaeological site is an art, verifying the cause of damage is science."

Bibliography

Ambrasyes, N. N., 2006. Earthquakes and archaeology. *Journal of Archaeological Science*, **33**, 108–1016.

Buck, V., and Stewart, I., 2000. A critical reappraisal of classical and archaeological evidence for earthquakes in the Atalanti region, central mainland Greece. In: McGuire, W. G., Griffith, D. R., Handcock, P. L., and Stewart, I. (eds.), *The Archaeology of Geological Catastrophes*, Geological Society, London, Special Publications 171, pp. 33–44.

De Rossi, M. S., 1874. La basilica di Santa Petronilla presso Roma, testé discoperta, caduta per terremoto. *Bulleltino del Vulcanismo Italiano*, **1**, 62–65.
Ellenblum, R., Marco, S., Agnon, A., Rockwell, T., and Boas, A., 1998. Crusader castle torn apart by earthquake at dawn, 20 May 1202. *Geology*, **26**, 303–306.
Evans, A., 1928. The Palace of Minos, part II. MacMillan: London, 844 pp.
Galadini, F., Hinzen, K.-G., and Stiros, S., 2006. Archaeoseismology: methodological issues and procedure. *Journal of Seismology*, **10**, 395–414.
Guidoboni, E. (ed.), 1989. *I terremoti prima del Mille in Italia e nell'area mediterranea. Storia, Archeologia, Sismologia*, ING-SGA, Bologna, (Italy), 765 pp.
McGuire, W. J., Griffith, D. R., Hancock, P. L., and Stewart I. S. (eds.), 2000. *The Archaeology of Geological Catastrophes*, Geological Society Spec. Publ. no. 171, London, 417 pp.
Meghraoui, M., Gomez, F., Sbeinati, R., Van der Woerd, J., Mounty, M., Darkal, A. N., Radwan, Y., Layyous, I., Al-Najjar, H., Darawcheh, R., Hijazi, F., Al-Ghazzi, R., and Barazangi, M., 2003. Evidence for 830 years of seismic quiescence from palaeoseismology, archaeoseismology, and historical seismicity along the Dead Sea Fault in Syria. *Earth and Planetary Science Letters*, **210**, 35–52.
Reicherter, K., Michetti, A. M., and Silva, P. G. (eds.), 2009. *Palaeoseismology: Historical and Prehistorical Records of Earthquake Ground Effects for Seismic Hazard Assessment*. The Geological Society, London, Special Publications, 316, 324 pp.
Schliemann, H., 1881. Autobiographie des Verfassers und Geschichte seiner Arbeiten in Troja. In: *Ilios. Stadt und Land der Trojaner, Forschungen und Entdeckungen in der Troas und besonders auf der Baustelle von Troja*, Leipzig, 78, 26 pp.
Stiros, S. C., and Jones, R. E. (eds.), 1996. *Archaeoseismology*. British School at Athens, Fitch Laboratory Occasional Paper 7, 268 pp.

Cross-references

Absolute Age Determinations: Radiometric
Earthquakes, Intensity
Earthquakes, Strong-Ground Motion
Numerical Methods, Finite Element
Paleoseismology
Seismic Hazard

ARTIFICIAL WATER RESERVOIR TRIGGERED EARTHQUAKES

Harsh K. Gupta
National Geophysical Research Institute, Council of Scientific & Industrial Research (CSIR), Hyderabad, Andhra Pradesh, India

Definition and Introduction

Under certain suitable geological conditions, anthropogenic activity can trigger or induce earthquakes. The triggered/induced earthquakes are known to have occurred due to gold and coal mining, petroleum production, filling of artificial water reservoirs, high-pressure liquid injection into ground, and natural gas production. The largest scientifically accepted triggered earthquake of magnitude 6.3 occurred on December 10, 1967 in the vicinity of Koyna Dam near the west coast of India. It is debated whether the M 7 Gazli earthquakes of May 1976 and March 19, 1984 were induced due to the production of large quantities of gas at the Gazli Oil Field in Uzbekistan. There is an argument that the Sichuan, China, M 7.9 earthquake of May 12, 2008, that claimed over 80,000 human lives was triggered due to filling of the nearby Zipingpu reservoir. It has been also proposed that flooding of a river near San Andreas fault in California caused at least two M $\sim$ 6 earthquakes. A good account of triggered/induced seismicity can be found in a review by McGarr et al. (2002). Hudyma and Potvin (2005) has extensively dealt with mining-induced seismicity. Gupta (2002) has reviewed artificial water reservoir triggered seismicity.

Here we present cases of artificial water reservoir triggered earthquakes that occurred all over the world, with a special emphasis on earthquakes in the Koyna region near the west coast of India. This is a classical case where triggered earthquakes have been occurring since the impoundment of reservoir in 1962.

Triggered vis-à-vis induced earthquakes

For a long time, the adjectives "induced" and "triggered" were used interchangeably whenever one talked of artificially simulated earthquakes. McGarr and Simpson (1997) have addressed this question and suggested that it would be important to draw a distinction between the two. They proposed that the adjective "triggered seismicity" should be used only when a small fraction of stress change or energy associated with earthquakes is accounted for by the causative activity. The term 'induced seismicity' should be used where the causative activity is responsible for a substantial part of the stress change. In case of triggered seismicity, tectonic loading plays an important role. The stress-level changes associated with filling of some of the deepest artificial water reservoirs are only of the order of 1 MPa or so, whereas the stress drop associated with the earthquakes is much larger. Therefore, all cases of earthquakes occurring subsequent to filling of the artificial water reservoirs fall in the category of "triggered earthquakes," and hence it is appropriate to call it "reservoir triggered seismicity" (RTS).

Artificial water reservoir triggered earthquakes

Generation of hydroelectric power, flood control, and irrigation necessitates creation of huge artificial water reservoirs globally. Triggering of earthquakes was for the first time pointed out by Carder (1945) at Lake Mead in USA. Figure 1 depicts Lake Mead water levels and local seismicity for the period 1936 through 1944. The rise in water level and corresponding bursts of seismic activity are numbered. The correspondence is indeed remarkable. Damaging triggered earthquakes exceeding magnitude six occurred at Hsingfengkiang, China (1962); Kariba, Zambia–Zimbabwe border (1963); Kremasta, Greece (1966); and Koyna, India (1967). Koyna earthquake of M 6.3 that occurred on December 10, 1967 is so far the largest scientifically accepted

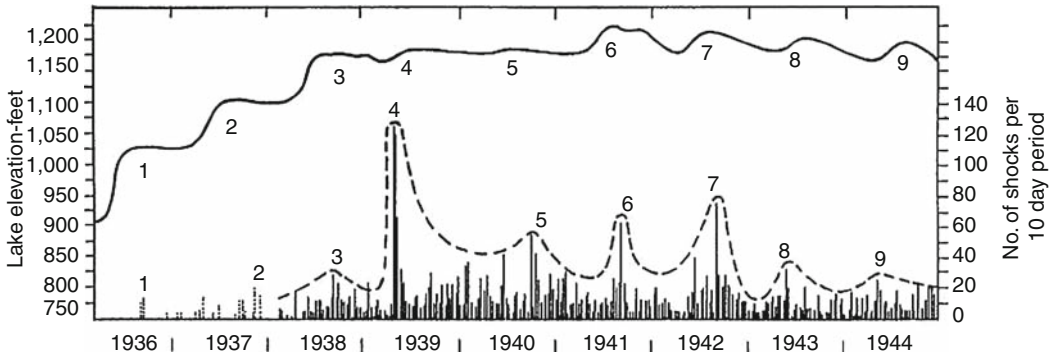

Artificial Water Reservoir Triggered Earthquakes, Figure 1 Lake Mead water levels and the local seismicity. For 1936 and 1937, only the felt shocks are plotted. The rises in water levels and the corresponding bursts of seismic activity are numbered. General trend of tremor-frequency variation is shown by dotted lines (After Carder, 1945).

triggered earthquake. It claimed over 200 human lives, injured about 1,500, and rendered thousands homeless. The occurrence and potential of triggered earthquakes has caused major modification of civil works and engineering projects. Anticipating a large triggered earthquake, the Hsingfengkiang Dam was strengthened twice before the occurrence of M 6.1 earthquake on March 20, 1962 (Shen et al., 1974). The disposal of waste fluid through injection into the ground at Rocky Mountain Arsenal had to be discontinued due to triggered earthquakes (Evans, 1966). The possibility of high magnitude triggered seismicity was responsible for terminating the Auburn Dam project in California (Allen, 1978). There is a general reluctance on the part of Engineering Community, globally, to accept the significance or even the existence of the phenomenon of triggered seismicity (Allen, 1982; Simpson and Leith, 1988). What Allen (1982) said a quarter century back: "From a purely economic point of view, not to speak of public safety, the problem of reservoir induced earthquakes deserves far more attention than it currently is receiving in most parts of the world", is still true.

Reservoir triggered seismicity (RTS): global distribution

Globally there are about 100 sites where RTS is reported to have occurred (Table 1). These could broadly be grouped in the following categories:

1. Sites where largest earthquake exceeded M 6.0 (4 sites)
2. Sites where the largest earthquake M was 5.0–5.9 (10 sites)
3. Sites where the largest earthquake M was 4.0–4.9 (29 sites)
4. Sites where the largest earthquake M was less than 4.0 (55 sites)

Table 1 gives a global list of artificial water reservoir sites where triggered earthquakes of M $\geq$ 4 are known to have occurred.

Important factors for RTS

Several studies examined the correspondence among possible correlates like rate of loading, highest water level reached, and the duration of retention of high water levels and the occurrence of RTS. The most important correlate is the depth of water column in the reservoir (Baecher and Keeney, 1982). Figure 2 demonstrates that when the water column depth exceeds 200 m, about one in five reservoirs have experienced RTS. A review of recent global examples gives support to this observation. It must also be noted that a reservoir with a water volume exceeding 1 km^3 and/or a water depth exceeding 100 m is called a large reservoir. Globally, there are more than one thousand such reservoirs and only a small percentage has evidenced RTS.

Common characteristics of RTS sequences

By early 1970s, over a dozen cases of RTS were known. In a couple of detailed studies, Gupta et al. (1972a, b) discovered several common characteristics of RTS sequences, which discriminated them from the normal earthquake sequences occurring in close by regions but not associated with reservoirs. These characteristics are:

1. In the earthquake frequency-magnitude relation ($\log N = A - b\,M$, where N is the number of earthquakes with magnitude $\geq$ M, and A and b are constants), the foreshock and aftershock *b* values of the RTS sequences are higher than the *b* values for natural earthquake sequences in the regions concerned, and the regional *b* values.
2. In addition to high *b* values, the magnitude ratio of the largest aftershock to the main shock is also high.
3. Aftershock activity decays slowly compared to normal earthquake sequences.
4. The foreshock–aftershock sequence pattern belongs to Type II of Mogi's Model (Mogi, 1963), where as the natural earthquake sequence pattern belongs to Type I of Mogi's Model.

Artificial Water Reservoir Triggered Earthquakes, Table 1 Reported cases of reservoir triggered seismicity (RTS) where M ≥ 4 earthquake occurs

Name of the dam/reservoir	Country	Height of dam (m)	Reservoir volume (10^6 m^3)	Year of impounding	Year of the largest earthquake	Magnitude/ intensity	References
Sites where earthquakes having magnitude ≥ 6.0 were triggered							
Hsinfengkiang	China (PRC)	105	13,896	1959	1962	6.1	1, 2, 3
Kariba Zambia	Zimbabwe	128	175,000	1958	1963	6.2	1, 2, 6
Koyna	India	103	2,780	1962	1967	6.3	1, 2, 4,5
Kremasta	Greece	160	4,750	1965	1966	6.2	1, 2, 4,5
Sites where earthquakes having magnitude between 5.0 and 5.9 were triggered							
Aswan	Egypt	111	1,64,000	1964	1981	5.6	2, 7
Benmore	New Zealand	110	2,040	1964	1966	5.0	1, 2, 8
Charvak	Uzbekistan	148	2,000	1971	1977	5.3	25
Eucumbene	Australia	116	4,761	1957	1959	5.0	2
Geheyan	China	151	3,400	1993	1997	VI	22a
Hoover	USA	221	36,703	1935	1939	5.0	1, 2, 10
Marathon	Greece	67	41	1929	1938	5.7	1, 2, 4,5
Oroville	USA	236	4400	1967	1975	5.7	2, 11
Srinagarind	Thailand	140	11,750	1977	1983	5.9	28
Warna	India	80	1,260	1985	1993	5.0	24
Sites where earthquakes having magnitude between 4.0 and 4.9 were triggered							
Aksombo Main	Ghana	134	148,000	1964	1964	V	2, 9
Bajina Basta	Yugoslavia	90	340	1966	1967	4.5–5.0	2, 5
Bhatsa	India	88	947	1981	1983	4.9	20
Bratsk	Russia	100	169		1996	4.2	22b
Camarillas	Spain	49	37	1960	1964	4.1	2, 4, 5
Canelles	Spain	150	678	1960	1962	4.7	2, 4, 5
Capivari–Cachoeira	Brazil	58	180	1970	1971	VI	17
Clark Hill	USA	60	3517	1952	1974	4.3	2, 12
Dahua	China (PRC)	74.5	420	1982	1993	4.5	26
Danjiangkou	China (PRC)	97	16,000	1967	1973	4.7	16
Foziling	China (PRC)	74	470	1954	1973	4.5	16
Grandwal	France	88	292	1959	1963	V	1, 2, 4,5
Hoa Binh	Vietnam	125		1988	1989	4.9	22c
Kastraki	Greece	96	1000	1968	1969	4.6	2
Kerr	USA	60	1505	1958	1971	4.9	1, 2, 9
Komani	Albania	130	1600	1985	1986	4.2	27
Kurobe	Japan	186	149	1960	1961	4.9	2,13
Lake Baikal	Russia					4–4.8a	23
Lake Pukaki	New Zealand	106	9000	1976	1978	4.6	21
Manicouagan 3	Canada	108	10,423	1975	1975	4.1	2
Marimbondo	Brazil	94	6150	1975	1975	IV	18
Monteynard	France	155	275	1962	1963	4.9	1, 2, 4,5
Nurek	Tadjikistan	317	1000	1972	1972	4.6	1, 2, 14
P. Colombia/ V.Grande	Brazil	40/56	1500/2300	1973–1974	1974	4.2	19
Piastra	Italy	93	13	1965	1966	4.4	2, 4, 5
Pieve de Cadore	Italy	116	69	1949	1950	V	2, 15
Shenwo	China (PRC)	50	540	1972	1974	4.8	16
Vouglans	France	130	605	1968	1971	4.4	2, 4, 5
Karun-III	Iran	185	2970	2005	2005	4.3	29

References: 1 = (Gupta and Rastogi, 1976); 2 = (Packer et al., 1979); 3 = (Shen et al., 1974); 4 = (Rothe, 1970, 1973); 5 = (Bozovic, 1974); 6 = (Gough and Gough, 1970b); 7 = (Toppozada, 1982); 8 = (Adams, 1974); 9 = (Simpson, 1976); 10 = (Carder, 1945); 11 = (Bufe et al., 1976); 12 = (Talwani, 1976); 13 = (Hagiwara and Ohtake, 1972); 14 = (Soboleva and Mamadaliev 1976); 15 = (Caloi, 1970); 16 = (Oike and Ishikawa, 1983); 17 = (Berrocal (personal communication), 1990); 18 = (Veloso et al., 1987); 19 = (Berrocal et al., 1984); 20 = (Rastogi et al., 1986a); 21 = (Reyners, 1988); 22a = (Chen et al., 1996), 22b = (Pavlenov and Sherman, 1996), 22c = (Tung,1996), 23 = (Djadkov, 1997), 24 = (Rastogi et al., 1997b); 25 = (Plotnikova et al., 1992); 26 = (Guang, 1995); 27 = (Muco, 1991b); 28 = (Chung and Liu, 1992); 29 = (Abas Kangi and Nematollah Heidari, 2008) (updated from Gupta 2002)

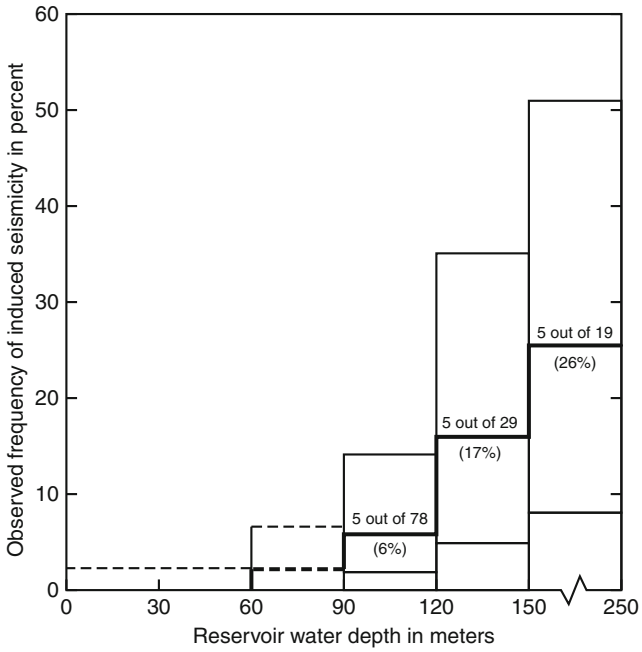

Artificial Water Reservoir Triggered Earthquakes, Figure 2 Height of water column is the most important correlate (After Stuart-Alexander and Mark, 1976).

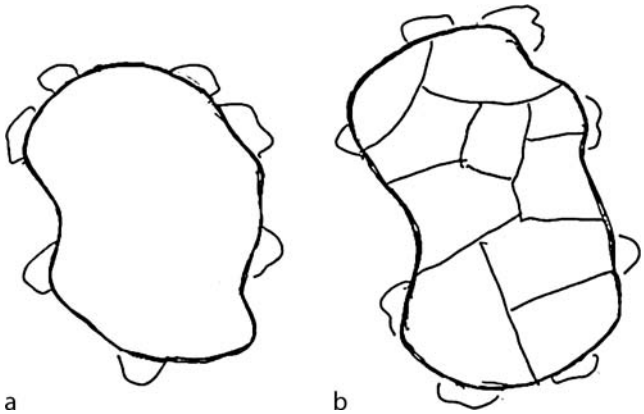

Artificial Water Reservoir Triggered Earthquakes, Figure 3 Impoundment of water reservoir increases heterogeneity. (**a**): Homogeneous rock volume before impoundment. (**b**): After impoundment. For **a**, earthquake sequence falls under Type 1 of Mogi's (1963) models: no foreshocks and a few aftershocks. For **b**, earthquake sequence falls under Type 2 of Mogi's (1963) models: considerable foreshock activity. For details see text.

The above-mentioned observations are governed by the mechanical properties of the media, and their deviation from the normal implies changes in these properties consequent to impoundment of the artificial water reservoir. It can be best illustrated by a sketch shown in Figure 3. "A" in this figure is a homogenous media rock volume. When the stress exceeds the strength of the rock, there would be a major event releasing most of the strain, followed by peripheral adjustment aftershocks. In such a sequence, there would not be any foreshocks before the major event. The aftershock activity would be over in a short time, the ratio of the largest aftershock to the main event would be low, and the *b* value would be low. This is typically the situation with the earthquake sequences in stable continental regions not associated with the reservoir loading. Due to filling of the water reservoir, the heterogeneity of the media increases ("B" in Figure 3), and the rock volume gets fragmented, and the accumulated stress is released by smaller rock volumes. In such a situation, the events would start occurring as and when the strength of an individual rock volume is exceeded. The main event would correspond to the largest rock volume and there would be events before it and after it, changing the pattern from Type I of Mogi's Model to Type II. The ratio of the magnitude of the largest aftershock to the main shock would be high, and the *b* value of the foreshock sequence as well as the aftershock sequence would be high. This is what is observed with RTS sequences.

Mechanism of triggered earthquakes

In the following we give a gist of major milestones in comprehending the phenomenon of triggered earthquakes.

The foundation of understanding the phenomenon of triggered earthquakes was laid by the study of the waste-fluid-injection-induced earthquakes in the vicinity of Rocky Mountain Arsenal Well near Denver, Colorado, USA, in early 1960s (Evans, 1966). There are three main effects of reservoir loading relevant to triggering of earthquakes as pointed out by Gough and Gough (1970b) and several others:

1. The elastic stress increase following filling of the reservoir
2. The increase in pore fluid pressure in saturated rocks, basically due to decrease in pore volume due to compaction, in response to increase in elastic stress
3. Pore-pressure changes related to fluid migration

Gough and Gough (1970a, b) provided the first definitive quantitative analysis of the role of the load of the water reservoir in triggering earthquakes at Lake Kariba. The role of reservoir load was also considered by Bell and Nur (1978) and Roeloffs (1988). They pointed out that reservoir-load-induced stresses at seismogenic depths are very small and can only perturb the ambient stress field. Gupta et al. (1972a, b) identified the rate of increase of reservoir water levels, maximum water levels reached, and the duration of retention of high water levels as factors affecting the frequency and magnitude of triggered earthquakes. The influence of pore fluid pressure in inducing earthquakes in very simple 1 D reservoir models was presented by Snow (1972). More sophisticated models were dealt by Withers and Nyland (1976), Bell and Nur

(1978), and Roeloffs (1988) based on Biot's (1941) consolidation theory, which later on is generalized by Rice and Cleary (1976) by recognizing that the fluids too may be compressible. Very interesting results related to modeling of pore-pressure diffusion have been reported for Acu Reservoir in Brazil (Do Nascimento et al., 2004).

Pore-pressure diffusion plays a very important role in the triggering of the earthquakes. However, there are a very few direct measurements of diffusivity, and it is mostly inferred from the temporal migration of seismicity. Talwani et al. (1999) have reported in situ measurements of hydrological diffusivity and Skempton's coefficient at the Bad Creek Reservoir in South Carolina, USA. At an observation well located 250 m away from the reservoir, a change in the water level of the well had a direct correspondence with the changes in the water level of the reservoir, initially with a delay of 98 h, which later stabilized at 72 h. This led to a frequency independent estimate of diffusivity of $\sim$0.076 $m^2\ s^{-1}$ and Skempton's coefficient of 0.66 for an undrained response of the reservoir. Later, Talwani et al. (2007) analyzed more than 90 case histories of triggered seismicity and found diffusivity to vary between 0.1 and 10 $m^2\ s^{-1}$. This range of diffusivity values corresponds to a range of intrinsic permeability between 5×10^{-16} and 5×10^{-14} m^2. Talwani et al. (2007) referred this range of the permeability of fractures as seismogenic permeability. Seismogenic permeability is an intrinsic property of fractures where pore-pressure diffusion is associated with seismicity.

The in situ measurements of physical properties and examination of physical mechanism controlling triggered seismicity at Monticello Reservoir, South Carolina, USA, provided the much needed field verification of the theoretical and model developments of concept of triggered seismicity (Zobak and Hickman, 1982). The effect of changes in lake levels and other derived parameters on triggered earthquakes have been dealt by Simpson and Negmatullaev (1981) for the Nurek Dam, and by Gupta (1983) for the Koyna Dam. The part played by pore-pressure diffusion in triggering earthquakes has been dealt by Talwani and Acree (1984/1985). The effect of inhomogeneities in rock properties on triggering earthquakes was addressed by Simpson and Narasimhan (1990).

Most of the theoretical models discussed the effect of pore fluid pressure in isotropic rocks. Chen and Nur (1992) point out that deviatory effects of pore fluid pressure in anisotropic rocks have wide applications in comprehending triggered seismicity, earthquake precursors, and aftershocks. This approach needs to be applied to a few cases of RTS.

Other interesting studies include the notion of fault stability as a measure of the interplay of frictional stresses mobilized and the resolved shear stresses acting on a fault Chander and Kalpna (1997). Kalpna and Chander (2000) have developed an algorithm for simulation of stresses and pore pressure for more realistic laterally finite 3D models of reservoirs.

Koyna, India

Koyna reservoir located close to the west coast of India continues to be the most significant site of triggered earthquakes. Earthquakes began to occur soon after the impoundment of the Shivaji Sagar Lake created by the Koyna Dam in 1962. So far, globally, the largest triggered earthquake of M 6.3 on December 10, 1967; 22 earthquakes of $M \geq 5$; about 200 earthquakes of $M \geq 4$; and several thousand smaller earthquakes have occurred in the region. Talking to residents in the region in the 1960s revealed that they had not experienced any earthquake in the region in their living memory. There is a seismic station operating at Pune, about 120 km away from Koyna. A scrutiny of the seismograms revealed no earthquakes that could be assigned to the Koyna region. Another water reservoir, Warna, was impounded in 1985. This reservoir is located 35 km SSE of Koyna (Figure 4). After the impoundment of Warna reservoir, the triggered activity got enhanced. For convenience, we shall call the Koyna and the Warna reservoirs region as the Koyna region. Major bursts of seismic activity associated with the Koyna reservoir occurred in 1967, 1993, 1980, 1993–1994, 2005, and 2009.

How long triggered earthquakes will continue at Koyna?

Koyna is indeed a unique site where triggered earthquakes have been occurring since the impoundment of the reservoir in 1962. Gupta et al. (2002) have examined in detail the question as to how long the triggered earthquakes would continue at Koyna. The maximum credible earthquake for the Indian shield region has been estimated to be M 6.8. It is hypothesized that the region between Koyna and Warna was stressed close to critical before the impoundment of the Koyna reservoir, and was capable of generating an M 6.8 earthquake. As demonstrated through the study of b values in earthquake magnitude-frequency relation, foreshock–aftershock patterns, the ratio of the magnitude of the largest aftershock to the main shock and the decay of aftershock activity in earthquake sequences at Koyna, the heterogeneity of the media has increased. None of the $M \sim 5$ earthquake has occurred at the same location. $M \sim 5$ earthquakes occur in Koyna region when the previous water maximum in the reservoir has been exceeded. Long time ago, Kaiser (1953) had reported that acoustic emission, under monotonically increasing stress, shows an appreciable increase after the applied stress exceeds the previously applied stress maxima. This approach has been successfully used by Yoshikawa and Mogi (1981) to estimate crustal stresses from cored samples. For the Nurek Dam also, it was reported that major triggered events occurred when water level in the reservoir reached the previous maximum and exceeded it (Simpson and Negmatullaev, 1981). Gupta et al. (2002) had concluded that as of 2002, about one-half of an M 6.8 earthquake energy has been released in the

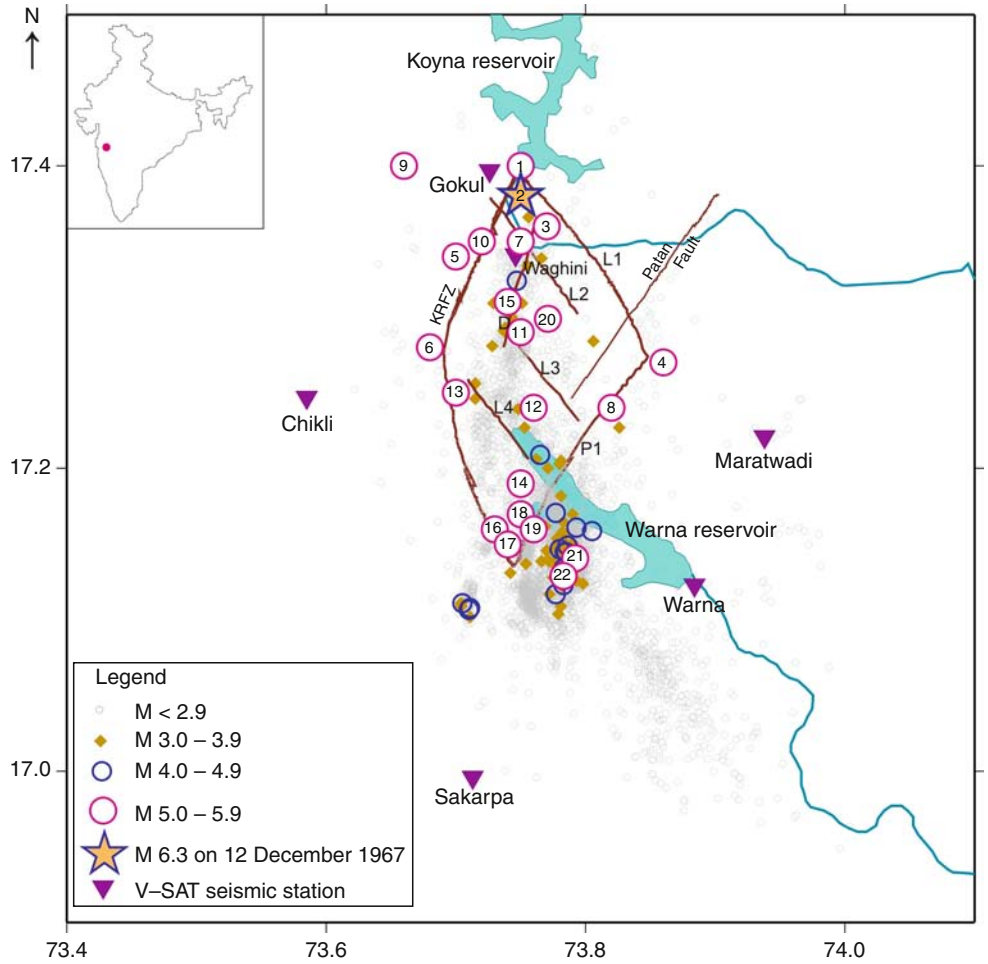

Artificial Water Reservoir Triggered Earthquakes, Figure 4 Earthquakes in Koyna region of Western India.

Artificial Water Reservoir Triggered Earthquakes, Table 2 Events preceding M $\geq$ 4.0 earthquakes in Koyna region

Main earthquake	Duration of nucleation period (h)	No. of events before the main earthquake				
		M 1.0–1.9	M 2.0–2.9	M 3.0–3.9	Largest earthquake	50 h prior to beginning of nucleation period
30th August 2005 M 4.8	110	13	8	0	2.6	2
13th November 2005 M 4.0	160	18	8	1	3.0	3
26th December 2005 M 4.2	150	22	8	0	2.9	6
17th April 2006 M 4.7	380	40	10	0	2.7	2

Koyna region, and the activity should continue for another 3–4 decades. Due to increase in heterogeneity, no fault segment long enough to generate an M > 6 earthquake is left intact; so an earthquake like the December 10, 1967, may not occur. The occurrence of M ~ 5 earthquakes would be governed by the fact whether the previous water maximum has been exceeded, and other factors such as the rate of loading, the highest water levels reached, and the duration of the retention of high water levels.

Short-term earthquake forecast at Koyna

A case was made that short-term earthquake forecast may be feasible at Koyna (Gupta, 2001). This was based on the fact that the shallow (depth $\leq$ 10 km) seismic activity in the vicinity of the Koyna is confined to an area of 20 $\times$ 30 km^2, and there is no other seismic source within 50 km radius. Every year, following the rainy season, the reservoirs get filled and there is an enhancement of seismic

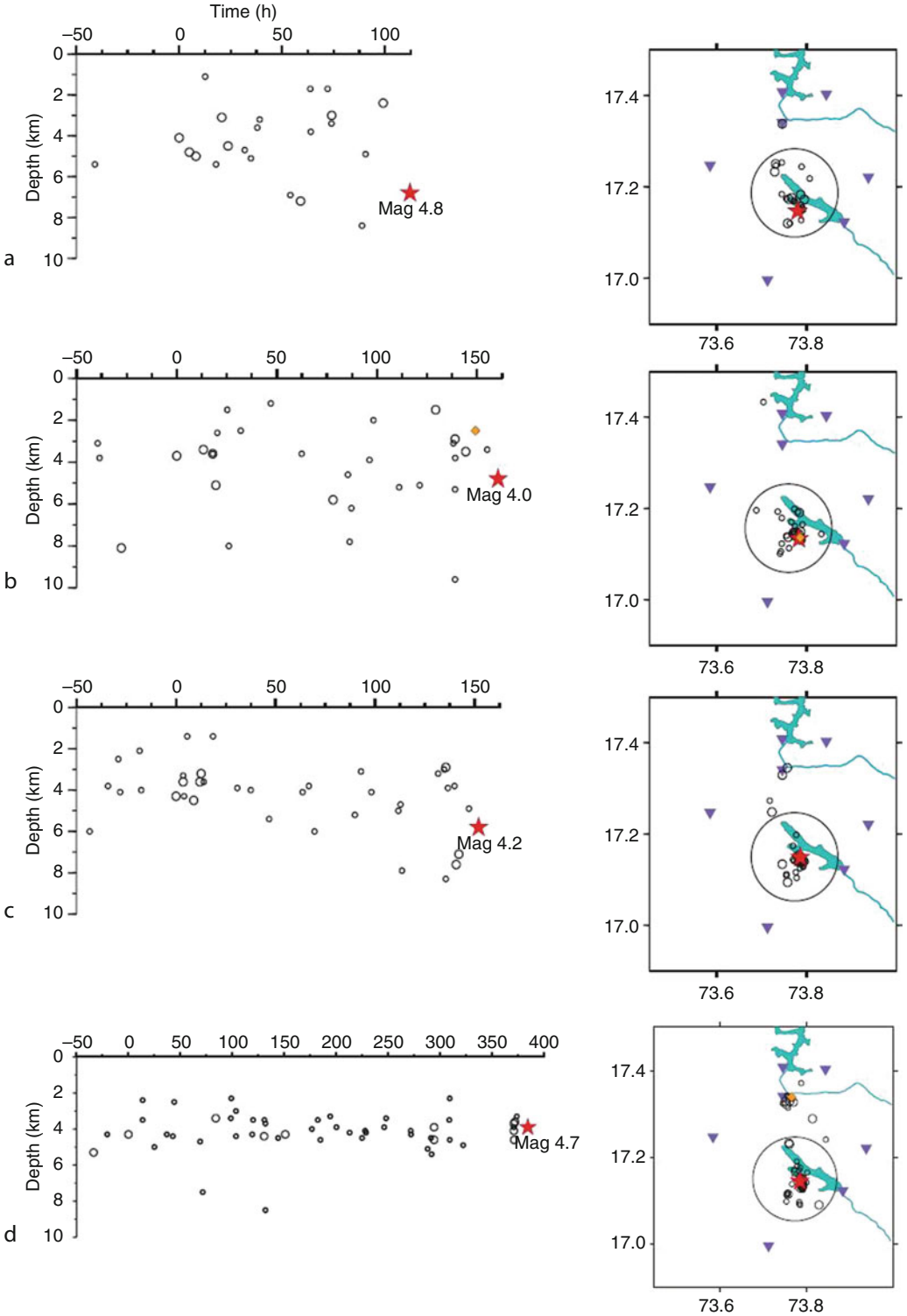

Artificial Water Reservoir Triggered Earthquakes, Figure 5 Seismic activity for the period 50 h before the start of nucleation till the occurrence of M $\geq$ 4 earthquakes in Koyna region during August 2005–April 2006. Foreshocks clustering before the main shocks in a region of 10 km radius (*Right*). Temporal distribution of events within the circle with the depth. ◦, ○, ◆ and ★ are events in M 1.0–1.9, 2.0–2.9 and 3.0–3.9 ranges, and main earthquake respectively (*Left*). Onset of identified nucleation period is given "0" time mark. Nucleation period lasted for 110, 160, 150 and 380 h for (**a**) 30th August, (**b**) 13th November and (**c**) 26th December 2005 (**d**) 17th April 2006 earthquakes respectively (Table 2).

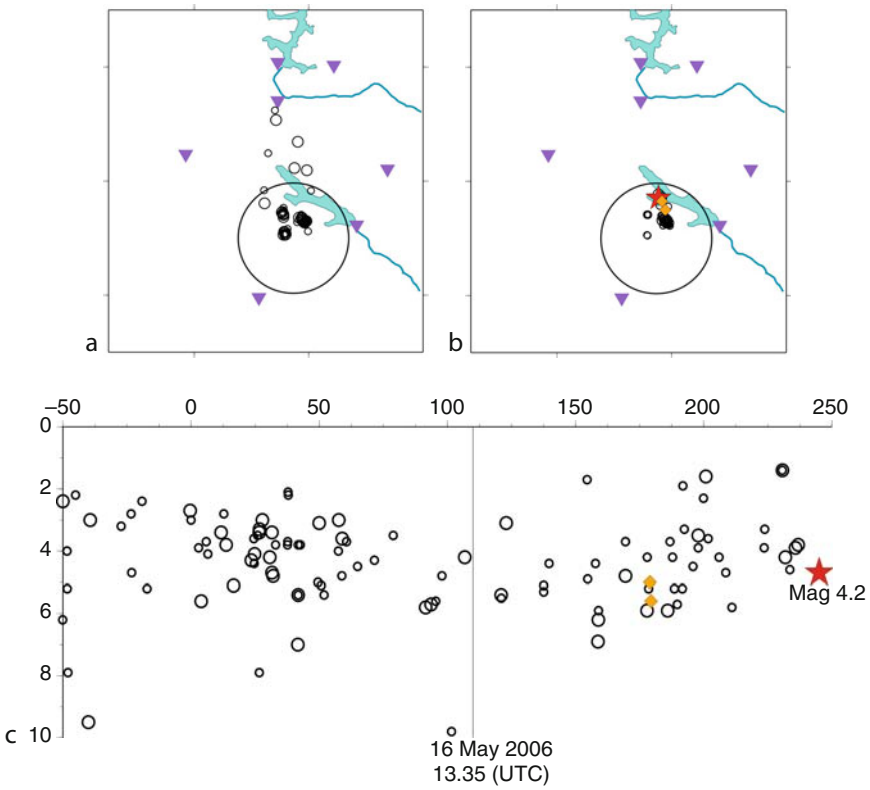

Artificial Water Reservoir Triggered Earthquakes, Figure 6 Symbols as in Figure 5. (**a**), Events that occurred during 107 h (11–16 May) preceding identification of nucleation. (**c**), Temporal-depth plot of the events within the 10 km radius circle. Nucleation was inferred to have started 107 h before, where 0 h is put on the time axis. (**b**), Seismic activity from 13:35 UTC on 16 May till the occurrence of the M4.2 earthquake on 21st May 2006, on the right side of (**c**).

activity. From among earthquake precursors, foreshocks are important and have a potential in forecasting earthquakes (Dodge et al., 1996; Helmestetter et al., 2003). Ohnaka (1992) has noted that immediate foreshock activity is a part of the nucleation process leading to main-shock dynamic rupture. Gupta et al. (2007) have reported successful earthquake forecast in Koyna based on identification of nucleation in real time. The seismic activity in the Koyna region is monitored by a closely spaced network of seven modern seismic stations. Table 2 from Gupta et al. (2007) is the learning phase where four earthquakes of M 4.0 to M 4.8 were found to be preceded by well-defined nucleation where several events occurred in a tight cluster of less than 10 km radius (Figure 5a–d). It was realized that if the formation of nucleation could be identified in real time before the occurrence of the main shock, it may be possible to make a short time forecast.

During the middle of May 2006, an interesting situation developed. The events in the Koyna region for the period 11–16th May, 2006, are depicted in Figure 6a (Gupta et al., 2007). By the afternoon of 16th May, 2006, some 50 events of $M \geq 1.0$, the largest being M 2.7, had occurred in the preceding 107 h in a small area, the focal depth being between 2 and 8 km. It was inferred that the region is going through a nucleation phase. Based on the experience of previous nucleation, the following forecast was made at 19:05 IST and communicated to the Editor of *Current Science*, Secretary, Ministry of Earth Sciences of the Government of India, and the President of the Geological Society of India: "On the basis of the data available from seven seismic stations operating in the Koyna region, we have identified a nucleation which started on 12th May 2006. This may lead to the occurrence of an $M \sim 4$ earthquake in the next 15 days. This shallow earthquake (focal depth less than 8 km) will occur within

Artificial Water Reservoir Triggered Earthquakes, Table 3 Forecast of 21st May, 2006, M 4.2 earthquake in Koyna on 16th May, 2006

	Forecast parameters	Occurrence
Epicenter	Within 10 km radius of 17.1°N, 73.8°E	17.171°N, 73.777°E
Magnitude	~4	4.2
Time	Within 15 days of 16th May 2006, i.e., until 31st May 2006	20:29:01 UTC On 21st May 2006
Focal depth	Less than 8 km	4.7 km

a radius of 10 km centered at 17.1°N, 73.8°E. On the basis of our previous experience of studying nucleation-preceding earthquakes in the Koyna region, we expect this earthquake to occur over the next 15 days time (till 31st May, 2006), with a 50% probability." An earthquake of M 4.2 occurred on 21st May. Table 3 gives the comparison of forecasted parameters and that of 21st May, 2006, earthquake. Since 2005, six similar short-term forecasts have been made in the Koyna region and all have come true.

Summary

In this article, we provide a thumbnail review of studies of global occurrence of artificial water reservoir triggered earthquakes, with a special emphasis on Koyna, India. Considering the small changes in the stress regime caused by filling of the deepest reservoirs compared to the stress drop of the associated earthquakes, it is appropriate to replace "reservoir-induced seismicity" by "reservoir triggered seismicity."

Koyna continues to be the most significant sight of RTS globally. The latest $M > 5$ earthquake occurred on December 12, 2009 (M 5.1).

At Koyna, earthquakes of M 4–5 are often preceded by well-defined clusters of foreshocks of $M \leq 3$, referred as nucleation that is found to last typically 100–400 h. Identification of nucleation in real time has led to successful short-term forecasts of $M \sim 4$ earthquakes.

Study of RTS provides exceptionally good input to comprehend physics of earthquakes, finding safer sites of creating artificial water reservoirs and bringing us closer to accurate short-term earthquake forecasts.

Bibliography

Allen, C. R., 1978. Evaluation of seismic hazard at the Auburn damsite. California, U.S. Bureau of Reclamation Report, Denver, p. 10.

Allen, C. R., 1982. Reservoir-induced earthquakes and engineering policy. *California Geology*, **35**, 248–250.

Baecher, B. G., and Keeney, R. L., 1982. Statistical examination of reservoir induced seismicity. *Bulletin. Seismological Society of America*, **72**, 553–569.

Bell, M. L., and Nur, A., 1978. Strength changes due to reservoir-induced pore pressure and stresses and application to Lake Oro-Berrocal. *Journal of Geophysical Research*, **83**, 4469–4483.

Biot, M. A., 1941. General theory of three-dimensional consolidation. *Journal of Applied Physics*, **12**, 155–164.

Carder, D. S., 1945. Seismic investigations in the Boulder Dam area, 1940–1944, and the influence of reservoir loading on earthquake activity. *Bulletin. Seismological Society of America*, **35**, 175–192.

Chander, R., and Kalpna, R., 1997. On categorizing induced and natural tectonic earthquakes near new reservoirs. *Engineering Geology*, 46.

Chen, Q., and Nur, A., 1992. Pore fluid pressure effects in an isotropic Rocks: mechanisms of induced seismicity and weak faults. *Pure and Applied Geophysics*, **139**, 463–480.

Do Nascimento, A. F., Cowie, P. A., Lunn, R. J., and Pearce, R. G., 2004. Spatio-temporal evolution of induced seismicity at Acu reservoir, NE Brazil. *Geophysical Journal International*, **158**, 1041–1052.

Dodge, D. A., Beroza, G. C., and Ellsworth, W. L., 1996. Detailed observations of California foreshock sequences: implications for the earthquake initiation process. *Journal of Geophysical Research*, **101**, 22371–22392.

Evans, M. D., 1966. Man made earthquakes in Denver. *Geotimes*, **10**, 11–17.

Gough, D. I., and Gough, W. I., 1970a. Stress and deflection in the lithosphere near Lake Kariba, 1. *Geophysical Journal*, **21**, 65–78.

Gough, D. I., and Gough, W. I., 1970b. Load induced earthquakes at Kariba. 2. *Geophysical Journal of the Royal Astronomical Society*, **21**, 79–101.

Gupta, H. K., 1983. Induced seismicity hazard mitigation through water level manipulation at Koyna, India: a suggestion. *Bulletin. Seismological Society of America*, **73**, 679–682.

Gupta, H. K., 2001. Short-term earthquake forecasting may be feasible at Koyna, India, Elsevier. *Tectonophysics*, **338**(3–4), 353–357.

Gupta, H. K., 2002. A review of recent studies of triggered earthquakes by artificial water reservoirs with special emphasis on earthquakes in Koyna, India. *Earth Science Reviews*, **58**, 279–310.

Gupta, H. K., Rastogi, B. K., and Narain, H., 1972a. Common features of the reservoir associated seismic activities. *Bulletin. Seismological Society of America*, **62**, 481–492.

Gupta, H. K., Rastogi, B. K., and Narain, H., 1972b. Some discriminatory Characteristics of earthquakes near the Kariba, Kremasta and Koyna artificial lakes. *Bulletin. Seismological Society of America*, **62**, 493–507.

Gupta, H. K., Mandal, P., and Rastogi, B. K., 2002. How long will triggered earthquakes at Koyna, India continue? *Current Science*, **82**(2), 202–210.

Gupta, H. K., et al., 2007. Earthquake forecast appears feasible at Koyna, India. *Current Science*, **93**(6), 843–848.

Helmestetter, A., Sornette, D., and Grasso, J. R., 2003. Mainshocks are aftershocks of conditional foreshocks: How do foreshock statistical properties emerge from aftershock laws? *Journal of Geophysical Research*, **108B**, 2046.

Hudyma, M. R., and Potvin, Y., 2005. Mining-Induced Seismicity in Underground Mechanised Hard rock Mines-Results of a World–Wide Survey. "*Seminar on Advanced Geomechanics in Mines*", 03 August 2005. Perth: Australian Centre for Geomechanics, pp. 47.

Kaiser, J., 1953. Erkenntnisse and Folgerungen aus der Messung von Gerauschen bei Zugbeanspruchung von metallischen Werkstoffen. *Archiv für das Eisenhüttenwesen*, **24**, 43–45 (in German).

Kalpna, and Chander, R., 2000. Green's function based stress diffusion solutions in the porous elastic half space for time varying finite reservoir loads. *Physics of the Earth and Planetary Interiors*, **120**, 93–101.

McGarr, A., and Simpson, D., 1997. Keynote lecture: A broad look at induced and triggered seismicity, "Rockbursts and seismicity in mines." In Gibowicz, S. J., and Lasocki, S. (eds.), *Proceedings of 4th International Symposium on Rockbursts and Seismicity in Mines Poland*, 11–14 Aug 1997. Rotterdam: A. A. Balkema Press, pp. 385–396.

McGarr, A., Simpson, D., and Seeber, L., 2002. Case histories of induced and triggered seismicity. *International Handbook of Earthquake and Engineering Seismology.* Orlando, FL: Academic Press, Vol. 81 A, pp. 647–661.

Mogi, K., 1963. Some discussions on aftershocks, foreshocks and earthquake swarms – The fracture of a semi infinite body caused by an inner stress origin and its relation to earthquake phenomena. *Bulletin. Earthquake Research Institute*, **41**, 615–658.

Ohnaka, M., 1992. Earthquake source nucleation: a physical model for short-term precursors. *Tectonophysics*, **211**, 249–278.

Rice, J. R., and Cleary, M. P., 1976. Some basic stress diffusion solutions for fluid-saturated elastic porous media with compressible constituents. *Reviews of Geophysics and Space Physics*, **14**(2), 227–242.

Roeloffs, E. A., 1988. Fault stability changes induced beneath a reservoir with cyclic variations in water level. *Journal of Geophysical Research*, **93**(B3), 2107–2124.

Shen, C., Chang, C., Chen, H., Li, T., Hueng, L., Wang, T., Yang, C., and Lo, H., 1974. Earthquakes induced by reservoir impounding and their effect on the Hsinfengkiang Dam. *Scientia Sinica*, **17**(2), 239–272.

Simpson, D. W., and Leith, W. S., 1988. Induced seismicity at Toktogul Reservoir, Soviet Central Asia. U.S. Geological Survey, No. 14-08- 0001-G1168, 32 pp.

Simpson, D. W., and Narasimhan, T. N., 1990. Inhomogeneities in rock Properties and their influence on reservoir induced seismicity. *Gerlands Beitrage zur Geophysik*, **99**, 205–219.

Simpson, D. W., and Negmatullaev, S. K., 1981. Induced seismicity at Nurek Reservoir, Tadjikistan, USSR. *Bulletin. Seismological Society of America*, **71**(5), 1561–1586.

Snow, D. T., 1972. Geodynamics of seismic reservoirs. Proceedings of Symposium on Percolation Through Fissured Rocks, Deutsche Gessellschaft fiir Erd- und Grundbau, Stuttgart, Germany, T2-J, pp. 1–19.

Stuart-Alexander, D. E., and Mark, R. K., 1976. Impoundment-induced seismicity associated with large reservoirs, U.S. Geological Survey Open-File Rept. pp. 76–770.

Talwani, P., and Acree, S., 1984/1985. Pore pressure diffusion and the mechanism of reservoir-induced seismicity. *Pure and Applied Geophysics*, **122**, 947–965.

Talwani, P., Cobb, J. S., and Schaeffer, M. F., 1999. In situ measurements of hydraulic properties of a shear zone in northwestern South Carolina. *Journal of Geophysical Research*, **104**(B7), 14993–15003.

Talwani, P., Chen, L., and Gahalaut, K., 2007. Seismogenic permeability, k_s. *Journal of Geophysical Research*, **112**, B07309, doi:10.1029/2006JB004665.

Withers, R. J., and Nyland, E., 1976. Theory for the rapid solution of ground subsidence near reservoirs on layered and porous media. *Engineering Geology*, **10**, 169–185.

Yoshikawa, S., and Mogi, K., 1981. A new method for estimating the crustal stress from cored rock samples; laboratory study in the case of uniaxial compression. *Tectonophysics*, **74**, 323–339.

Zoback, M. D., and Hickman, S., 1982. Physical mechanisms controlling induced seismicity at Monticello Reservoir, South Carolina. *Journal of Geophysical Research*, **87**, 6959–6974.

Cross-references

Earthquake Precursors and Prediction
Earthquake Prediction, M8 Algorithm
Earthquake, Aftershocks
Earthquake, Foreshocks
Earthquakes, Energy
Seismicity, Intraplate
Seismological Networks

http://www.springer.com/978-90-481-8701-0

Encyclopedia of Solid Earth Geophysics
NGRI, D. (Ed.)
2011, LXXIV, 1539 p. In 2 volumes, not available separately., Hardcover
ISBN: 978-90-481-8701-0